Stem Cell Reports
Article

ISSCR

OPEN ACCESS

LincU Preserves Naïve Pluripotency by Restricting ERK Activity in Embryonic Stem Cells

Zeyidan Jiapaer,[1,4] Guoping Li,[1,4] Dan Ye,[1] Mingliang Bai,[1] Jianguo Li,[1] Xudong Guo,[1,2] Yanhua Du,[1] Dingwen Su,[1] Wenwen Jia,[1] Wen Chen,[1] Guiying Wang,[1] Yangyang Yu,[1] Fugui Zhu,[1] Xiaoping Wan,[3] and Jiuhong Kang[1,*]

[1]Clinical and Translational Research Center of Shanghai First Maternity & Infant Health Hospital, Shanghai Key Laboratory of Signaling and Disease Research, Collaborative Innovation Center for Brain Science, School of Life Sciences and Technology, Tongji University, 1239 Siping Road, Shanghai 200092, PR China
[2]Institute of Regenerative Medicine, East Hospital, Tongji University School of Medicine, Shanghai, PR China
[3]Department of Gynecology, Shanghai First Maternity and Infant Hospital, Tongji University School of Medicine, Shanghai, PR China
[4]Co-first author
*Correspondence: jhkang@tongji.edu.cn
https://doi.org/10.1016/j.stemcr.2018.06.010

SUMMARY

Although the functional roles of long noncoding RNAs (lncRNAs) have been increasingly identified, few lncRNAs that control the naïve state of embryonic stem cells (ESCs) are known. Here, we report a naïve-state-associated lncRNA, LincU, which is intrinsically activated by *Nanog* in mESCs. LincU-deficient mESCs exhibit a primed-like pluripotent state and potentiate the transition from the naïve state to the primed state, whereas ectopic LincU expression maintains mESCs in the naïve state. Mechanistically, we demonstrate that LincU binds and stabilizes the DUSP9 protein, an ERK-specific phosphatase, and then constitutively inhibits the ERK1/2 signaling pathway, which critically contributes to maintenance of the naïve state. Importantly, we reveal the functional role of LincU to be evolutionarily conserved in human. Therefore, our findings unveil LincU as a conserved lncRNA that intrinsically restricts MAPK/ERK activity and maintains the naïve state of ESCs.

INTRODUCTION

Early embryonic development involves dynamic cellular conversion events that are characterized by dramatic changes in both extrinsic signaling pathways and intrinsic epigenetic and transcriptional programs (Young, 2011). Preimplantation blastocysts have the capacity to differentiate into both somatic cells and germ cells and are thus considered to display a naïve pluripotent state (Bradley et al., 1984; Leitch and Smith, 2013). Upon implantation, the inner cell mass (ICM) develops into the epiblast, which is characterized by the incipient expression of germ layer markers and disintegration of the naïve pluripotency network, considered to be a primed pluripotent state (Nichols and Smith, 2009). In addition, the inaccessibility of these transient cell populations *in vivo* further restricts the study of this process directly. Fortunately, mouse embryonic stem cells (mESCs), derived from the ICM, provide a versatile model for studying this transient process *in vitro* (Evans and Kaufman, 1981; Martin, 1981). When cultured *in vitro*, mESCs exhibit two distinct pluripotent states, the original naïve state and the primed state (epiblast-like cells), which display distinct morphological, transcriptional, and epigenetic profiles (Hackett and Surani, 2014; Kalkan and Smith, 2014). Naïve-state clones show round morphology while primed-state clones are flat, similar to human ESCs (hESCs) (Nichols and Smith, 2009; Tesar et al., 2007). *Nanog*, *Klf2* and *Esrrb* have been defined as the core transcription factors that determine the naïve state of mESCs (Dunn et al., 2014; Festuccia et al., 2012; Stuart et al., 2014), whereas *Brachyury*, *Fgf5*, and *Eomes* are unique genes expressed in the primed state (Nichols and Smith, 2009). The transition from the naïve state to the primed state is accompanied by global upregulation of H3K27me3 and DNA methylation (Marks et al., 2012). Further understanding the core regulatory network that dominates these two pluripotent states will be pivotal to studying preimplantation embryonic development and applying this knowledge to regenerative medicine.

Signaling pathways are commonly acknowledged as the main extrinsic factors that trigger the transition between naïve and primed pluripotent states (Hackett and Surani, 2014; Kunath et al., 2007). The leukemia inhibitory factor (LIF) and bone morphogenetic protein 4 (BMP4) signaling pathways have been shown to be critical for the self-renewal of naïve-state stem cells but are dispensable for the primed state (Niwa et al., 2009; Yoshida et al., 1994). Additionally, activation of the ERK1/2 signaling pathway triggers the transition from the naïve state to the primed state, and this pathway collaborates with the ACTIVIN/NODAL signaling pathway to maintain the primed state (Brons et al., 2007; Hackett and Surani, 2014; Ogawa et al., 2007). Interestingly, LIF also induces the activation of the ERK1/2 signaling pathway in the naïve pluripotent state regardless of the primarily activated LIF signaling pathway (Nichols et al., 2001). In addition, while ERK1/2

signaling drives lineage priming in mESCs, it is also required for the maintenance of self-renewal in hESCs (Greber et al., 2010). Moreover, the evolutionarily conserved fibroblast growth factor (FGF)/ERK signaling pathway has been reported to control a multitude of early embryonic developmental processes, including proliferation, survival, migration, metabolism, and differentiation (Roskoski, 2012). All of these observations underscore the importance of the ERK1/2 signaling pathway in stem cell fate decisions. Strikingly, maintenance of a homogeneous naïve pluripotent state is enabled by the elimination of differentiation-inducing signals from the ERK1/2 signaling pathway (Nichols et al., 2009; Ying et al., 2008). Therefore, fine-tuning of ERK1/2 activity is critical for determining the pluripotent state of stem cells. Recently, exogenous BMP4 was reported to steadily attenuate ERK1/2 activity by upregulating the expression of the pluripotency-specific protein dual-specificity phosphatase 9 (*Dusp9*), which binds to ERK1/2 and inhibits its phosphorylation in the naïve pluripotent state (Li et al., 2012). However, the intrinsic modifiers that modulate the activity of ERK1/2 signaling pathway are rarely uncovered.

Long noncoding RNAs (lncRNAs), with lengths more than 200 bp, are more versatile in distinct biological processes, accounting for their higher-ordered structures and flexible expression patterns (Batista and Chang, 2013; Guttman and Rinn, 2012; Rinn and Chang, 2012). Based on their genomic location, lncRNAs can be classified as sense, antisense, bidirectional, intronic, or intergenic (lincRNA) (Fatica and Bozzoni, 2014). By functioning as molecular scaffolds, lncRNAs participate in the regulation of gene expression and the post-translational modification of proteins, including ubiquitination and phosphorylation (Nagano et al., 2008; Pandey et al., 2008; Taniue et al., 2016; Wang et al., 2014). The p53-induced lincRNA-p21 represses the translation of CTNNB1 and JUNB by directly interacting with their mRNAs (Yoon et al., 2012). Furthermore, linc00673 can reinforce the interaction between PTPN11 and PRPF19 and promote the ubiquitination and degradation of PTPN11 (Zheng et al., 2016). A previous study in dendritic cells revealed that the lincRNA lnc-DC could directly interact with STAT3 and sustain its phosphorylation at tyrosine-705 by preventing SHP1-mediated dephosphorylation (Wang et al., 2014). Recently, lncRNAs that collaborate with epigenetic remodeling complexes to directly regulate gene expression for the maintenance of pluripotency and lineage commitment in pluripotent stem cells have been discovered (Dinger et al., 2008; Guttman et al., 2011). Nevertheless, lncRNAs involved in the regulation of core signaling pathway activity in pluripotent stem cells remain largely unexplored.

Here, we report a naïve mESC specifically expressed lincRNA, LincU (previously referred as linc1483 [Guttman et al., 2011]), whose deficiency promotes the transition from naïve state to primed state, and its overexpression inhibits this process. Mechanistically, we found that LincU specifically restricts the activity of the mitogen-activated protein kinase (MAPK)/ERK signaling pathway by binding and stabilizing the ERK-specific phosphatase DUSP9. Our results suggest that LincU acts as an intrinsic inhibitor of MAPK/ERK signaling and critically controls the naïve pluripotent state of mESCs.

RESULTS

LincU Is Both Essential and Sufficient for Maintaining the Naïve Pluripotency of mESCs

Naïve pluripotency holds great promise for the clinical application of pluripotent stem cells (Batista and Chang, 2013). Although thousands of lncRNAs have been identified and integrated into the pluripotency regulation network (Guttman et al., 2011), functional lncRNA that plays a pivotal role in the maintenance of naïve pluripotency has rarely been found. As *Nanog* is considered a core element in naïve-state maintenance (Chambers et al., 2003, 2007; Mitsui et al., 2003) we found that *Nanog* can bind the promoter region of LincU, which is located on chromosome 16 (9,133,405–9,138,147) (mm9) (Murakami et al., 2016). Similar to that of *Nanog*, the expression pattern of LincU is dramatically and rapidly downregulated after LIF withdrawal (Figure S1A). Thus, to identify the functional role of LincU in the maintenance of naïve pluripotency, we assessed the expression levels of LincU in the mESCs at different pluripotent states, including those at the primed pluripotent state (sustained with basic FGF [bFGF] and activin A, bFGF + activin A), naïve pluripotent state (maintained with LIF and 2i, LIF + 2i), and heterogeneous pluripotent state (cultured in medium supplemented with LIF and fetal bovine serum [FBS], LIF + FBS). As expected, the naïve pluripotency-specific genes *Rex1*, *Esrrb*, *Nanog*, and *Tcl1* are highly expressed in the heterogeneous pluripotent state and even more highly expressed in the naïve pluripotent state, while the primed-state genes *Fgf5*, *Dnmt3b*, *T*, and *Eomes* together with the developmental genes *Nestin*, *Mixl l*, *N-cad*, and *Gata4* are highly expressed in the primed pluripotent state (Figure 1A). Compared with ESCs cultured in bFGF + activin A and LIF + FBS, ESCs cultured in LIF + 2i showed higher expression level of LincU (Figure 1A), which is in accordance with the expression patterns of naïve pluripotency-specific genes, indicating a potentially pivotal role of LincU in the maintenance of the naïve pluripotent state.

Employing a nucleocytoplasmic separation assay, we observed that the LincU transcripts were abundant in the cytoplasm of naïve-state mESCs (Figure S1B). Thus, we

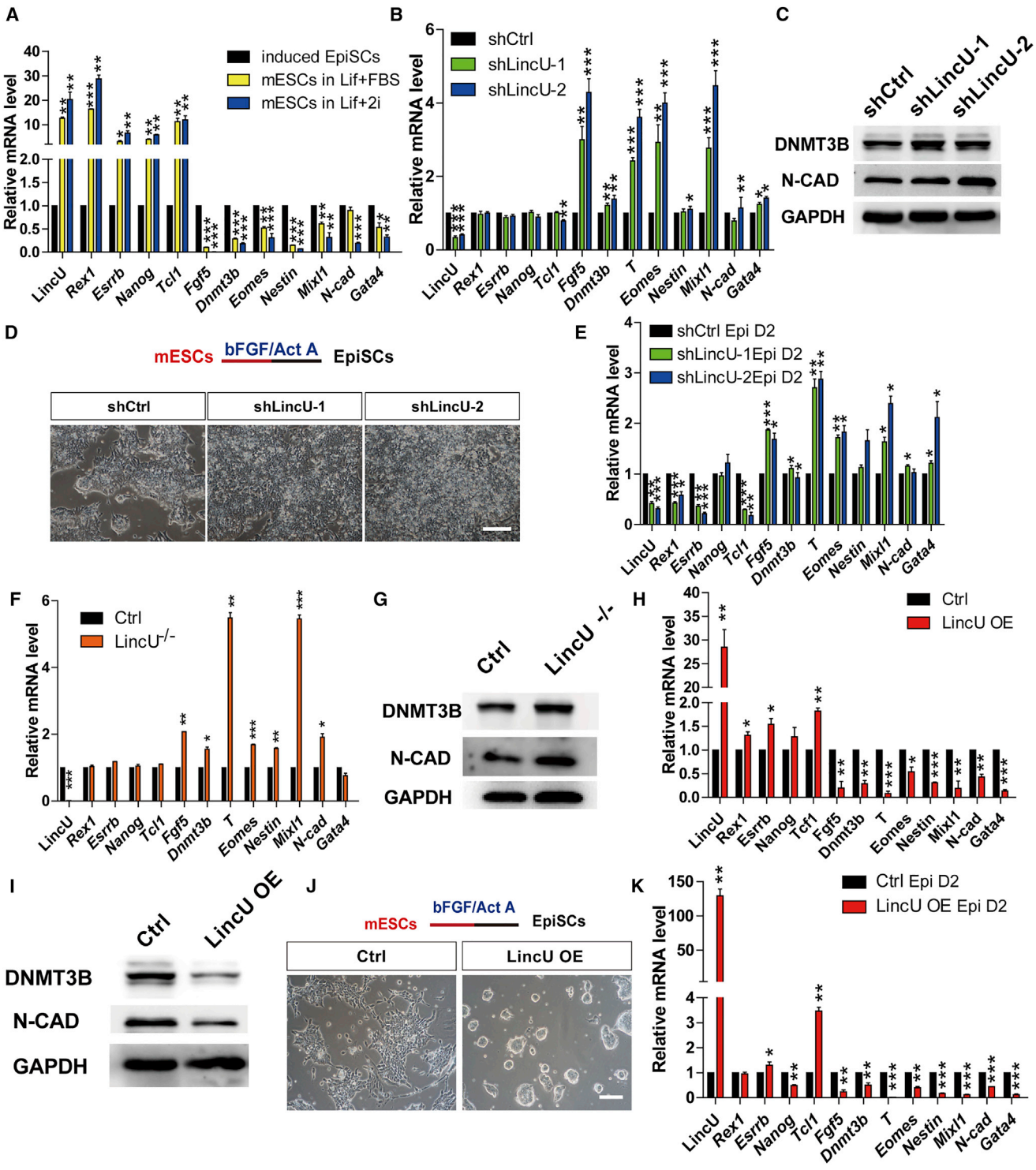

Figure 1. LincU Is Both Essential and Sufficient for Maintaining the Naïve Pluripotency of mESCs

(A) LincU is highly expressed in the heterogeneous pluripotent state and even more highly expressed in the naïve pluripotent state. Data are shown as the mean ± SEM (n = 3). *p < 0.05, **p < 0.01, ***p < 0.001, t test.

(B and C) shLincU mESCs exhibit a primed-like state when cultured in LIF + FBS medium, as shown by qPCR (B) and western blot (C) analysis of primed-state-related and developmental genes. Data are shown as the mean ± SEM (n = 3). *p < 0.05, **p < 0.01, ***p < 0.001, t test.

(legend continued on next page)

designed two efficient short hairpin RNAs (shRNAs) that target LincU transcripts to knock down its expression (shLincU-1 and shLincU-2) in mESCs via a lentivirus delivery system; a scrambled shRNA (shCtrl) served as the negative control. When cultured in LIF + FBS medium, mESCs fluctuate between the naïve and primed pluripotent states, which is termed the heterogeneous pluripotent state (Festuccia et al., 2012), and provides a more accessible platform to study the transition between the naïve and primed states. After maintaining shLincU and shCtrl mESCs in this serum-containing medium, shLincU mESCs exhibited a primed-like pluripotent state, which was characterized by higher expression levels of primed-state-specific genes, including *Fgf5*, *Dnmt3b*, *T*, *Eomes*, *Mixl1*, and *N-cadherin*, although LincU knockdown had no apparent influence on the expression of naïve-state-related genes (Figure 1B). Western blot also confirmed the elevated expression levels of primed-state-specific proteins (Figures 1C and S1C). Increased expression level of DNMT3B, a DNA methyltransferase, will enhance DNA methylation, which is well known to be a dominant feature of the primed pluripotent state (Borgel et al., 2010).

To validate the primed-like pluripotent state of LincU knockdown mESCs, we directly induced these mESCs to enter the primed pluripotent state by applying N2B27 + bFGF + activin A medium (Hayashi et al., 2011). As expected, LincU knockdown mESCs exhibited accelerated epiblast induction compared with shCtrl mESCs, as determined by more notable epiblast-like morphology, decreased expression of naïve-state-related genes, and increased expression of primed-state-related genes after 2 days of induction (Figures 1D and 1E). Furthermore, when we replated the induced primed pluripotent cells (cultured in N2B27 + activin A + FGF2) into LIF + FBS medium, LincU knockdown cells failed to form alkaline phosphatase (AP)-positive colonies (Figures S1D and S1E) (Karwacki-Neisius et al., 2013). These data demonstrated that LincU knockdown mESCs exhibit a primed-like pluripotent state.

To further confirm the functional role of LincU in the maintenance of naïve pluripotency, we directly generated LincU$^{-/-}$ mESCs via CRISPR/Cas9-mediated genome deletion (Li et al., 2017). Knockout efficiency was validated by genomic DNA PCR (Figure S1F) and qPCR (Figure 1F). Similarly, LincU$^{-/-}$ mESCs expressed higher levels of primed-state-specific genes when maintained in a heterogeneous pluripotent state (Figures 1F, 1G, and S1G). Moreover, we evaluated whether LincU$^{-/-}$ cells could contribute to chimeras and found that mESCs lacking LincU failed to form chimeras, thereby demonstrating that LincU-deficient mESCs have lost naïve pluripotency (Figures S2A and S2B). Additionally, we performed the teratoma formation assay and our results showed that LincU$^{-/-}$ mESCs formed larger teratomas with higher expression levels of primed-state and lineage-specific genes (Figures S2C and S2D). These results demonstrated that LincU is required for maintaining the naïve pluripotency of mESCs.

Next, we built the LincU-overexpressing mESCs by integrating CAG promoter-driven LincU expression into the Rosa26 locus using CRISPR/Cas9-mediated homologous recombination (Li et al., 2017). After confirming the constitutive overexpression of LincU transcripts, we found that LincU-overexpressing mESCs expressed lower expression levels of primed-state-related and developmental genes than control mESCs when cultured in LIF + FBS medium (Figure 1H). Additionally, a slight increase in the expression of naïve-state-related genes was observed (Figure 1H). Western blot assay also verified the decreased DNMT3B and N-CADHERIN protein levels (Figures 1I and S2E). These observations indicated that LincU-overexpressing mESCs exhibit a naïve-like pluripotent state. To further confirm this hypothesis, we induced control and LincU-overexpressing mESCs to differentiate to the primed pluripotent state. Notably, the LincU-overexpressing mESCs failed to transit to the primed state, as shown by a naïve-state morphology and a much lower expression level of primed-state-related genes than that in control mESCs (Figures 1J and 1K). Moreover, the induced EpiSCs derived from LincU-overexpressing mESCs were still able to form AP-positive colonies after being replated into LIF + FBS medium (Figures S2F and S2G), showing that overexpression of LincU severely disrupted

(D and E) LincU knockdown accelerates the epiblast induction process as shown by microscopy (D) and qPCR (E) analysis of epiblast cells induced for 2 days. Data are shown as the mean ± SEM (n = 3). *p < 0.05, **p < 0.01, ***p < 0.001, t test. Scale bar, 100 μm.

(F and G) LincU$^{-/-}$ mESCs express higher levels of primed-state-specific genes and developmental genes when cultured in LIF + FBS medium, as shown by qPCR (F) and western blot (G) analysis. Data are shown as the mean ± SEM (n = 3). *p < 0.05, **p < 0.01, ***p < 0.001, t test.

(H and I) LincU-overexpressing mESCs express lower levels of primed-state-related genes and developmental genes when cultured in LIF + FBS medium, as shown by qPCR (H) and western blot (I) analysis. Data are shown as the mean ± SEM (n = 3). *p < 0.05, **p < 0.01, ***p < 0.001, t test.

(J and K) LincU-overexpressing mESCs fail to differentiate into the primed pluripotent state, as shown by microscopy (J) and qPCR (K) analysis of day-2 induced epiblast cells. Data are shown as the mean ± SEM (n = 3). *p < 0.05, **p < 0.01, ***p < 0.001, t test. Scale bar, 100 μm.

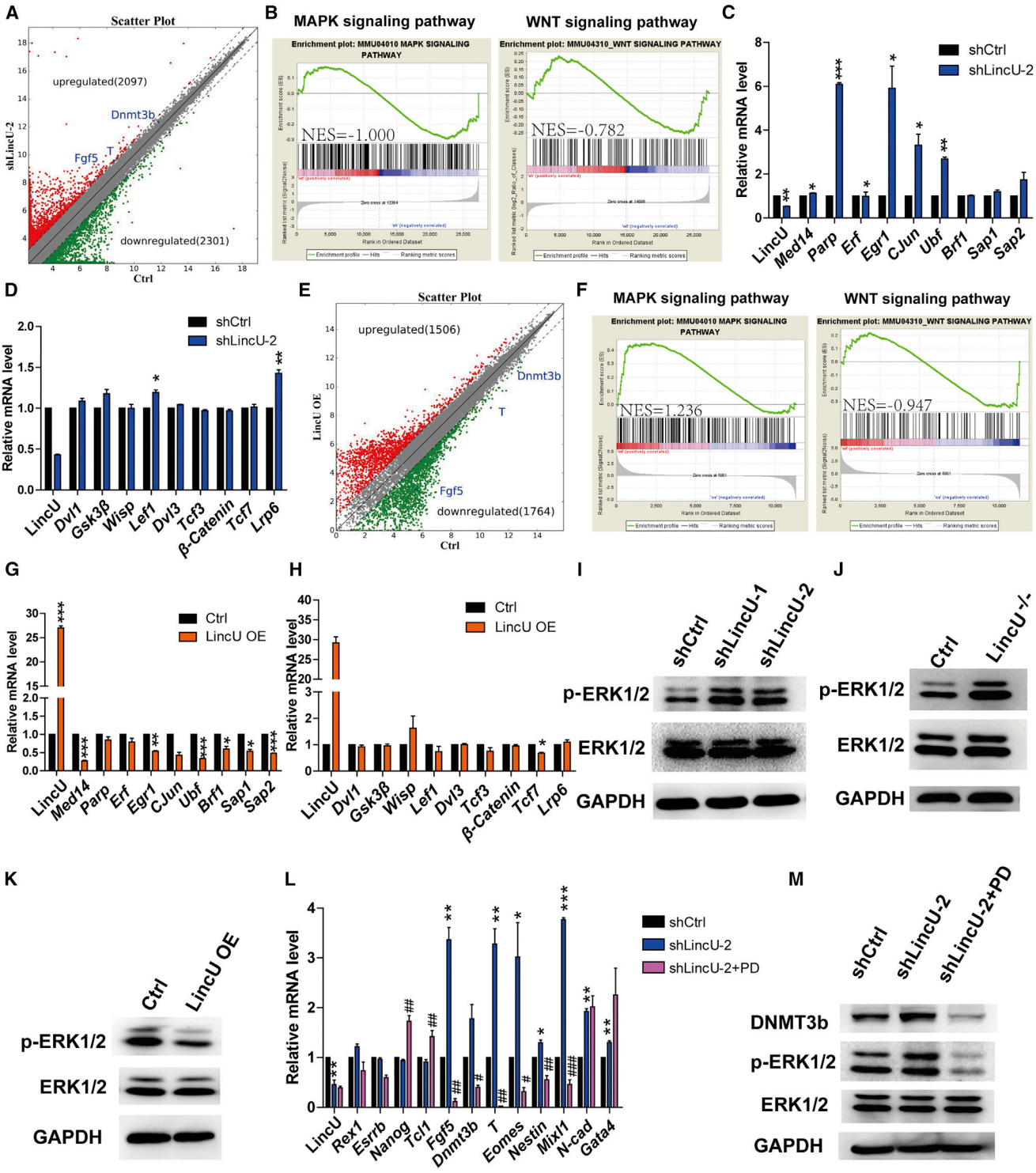

Figure 2. LincU Specifically Inhibits the MAPK-ERK Signaling Pathway

(A) Scatterplots of global gene expression according to microarray data for shLincU-2 mESCs versus shCtrl mESCs. The gray dashed lines delineate the boundaries of a 2-fold change in gene expression. Upregulated genes are highlighted in red and downregulated genes are shown in green.

(B) GSEA of the MAPK and WNT signaling pathways in shLincU-2 mESCs versus shCtrl mESCs. NES represents the normalized enrichment scores in each category.

(legend continued on next page)

the transition from the naïve pluripotent state to the primed pluripotent state. Similarly, we performed the teratoma formation assay with control and LincU-overexpressing mESCs, whereby LincU overexpression resulted in a smaller teratoma size and lower expression level of lineage-specific genes than those in control mESCs (Figures S2H and S2I). These *in vivo* results further confirmed that LincU-overexpressing mESCs maintain a naïve-like pluripotent state that is resistant to the initiation of differentiation. Collectively, these results demonstrated that LincU is both essential and sufficient for maintaining the naïve pluripotency of mESCs.

LincU Specifically Inhibits the MAPK-ERK Signaling Pathway

To determine the mechanism underlying LincU-induced key phenotypes in mESCs, we performed global transcriptome analysis of both LincU knockdown and LincU-overexpressing mESCs, which were maintained in the heterogeneous pluripotent state. Consistently, primed-state-related genes were upregulated upon LincU knockdown and downregulated upon LincU overexpression (Figures 2A and 2E). In addition, gene ontology analysis of these differentially expressed genes showed that LincU deficiency led to significant upregulation of functional terms related to *in utero* embryonic development, whereas LincU overexpression notably downregulated these functional terms (Figures S3A and S3B). Importantly, KEGG (Kyoto Encyclopedia of Genes and Genomes) pathway analysis of the downregulated genes in LincU-overexpressing mESCs showed that these genes are significantly enriched in the MAPK signaling pathway (Figure S3C). Furthermore, we performed gene set enrichment analysis (GSEA) and analyzed the normalized enrichment scores (NES) for two key signaling pathways that are involved in naïve-state reprogramming and maintenance: the MAPK/ERK and WNT signaling pathways. Our results indicated that MAPK signaling, but not WNT signaling, was significantly affected in both LincU knockdown and LincU-overexpressing mESCs (Figures 2B and 2F). We further examined the expression level of downstream genes of the WNT and MAPK/ERK signaling pathways, and our data indicated that LincU was negatively correlated with the expression level of MAPK/ERK downstream genes, but not the downstream genes of the WNT signaling pathway (Figures 2C, 2D, 2G, and 2H), which suggested that the activity of MAPK/ERK signaling pathway was affected by LincU expression manipulation.

To validate the sequential changes of MAPK/ERK signaling pathway activity after modifying the expression of LincU, we examined the level of ERK1/2 phosphorylation in LincU knockdown, LincU knockout, and LincU-overexpressing mESCs. Consistently, the level of ERK1/2 phosphorylation was markedly increased by LincU knockdown or knockout and dramatically decreased by LincU overexpression (Figures 2I–2K and S3D–S3F). Meanwhile, we also observed a negative correlation between the LincU expression level and the level of ERK1/2 phosphorylation in the teratomas derived from these three groups of mESCs (Figures S3G–S3J). Moreover, treatment with a potent MAPK inhibitor, PD0325901, significantly compromised the LincU knockdown-induced upregulation of primed-state-related genes and increased the level of ERK1/2 phosphorylation and DNMT3B protein (Figures 2L, 2M, and S3K). In conclusion, these results proved that LincU specifically inhibits MAPK/ERK signaling activity in mESCs, thereby elucidating the role of LincU in maintaining the naïve state.

LincU Stabilizes the ERK-Specific Phosphatase DUSP9 in mESCs

Direct competition between phosphorylation and dephosphorylation has been proposed as a major mechanism underlying extracellular stimulation and has been documented

(C and D) LincU knockdown increases the expression of downstream genes of the MAPK signaling pathway (C) but barely affects the expression level of WNT target genes (D). Data are shown as the mean ± SEM (n = 3). *p < 0.05, **p < 0.01, ***p < 0.001, t test.

(E) Scatterplots of global gene expression according to microarray data for LincU-overexpressing mESCs versus Ctrl mESCs. The gray dashed lines delineate the boundaries of a 2-fold change in gene expression. Upregulated genes are highlighted in red and downregulated genes are shown in green.

(F) GSEA of the MAPK and WNT signaling pathways in LincU-overexpressing mESCs versus Ctrl mESCs. NES represents the normalized enrichment scores in each category.

(G and H) LincU overexpression decreases the expression of the downstream genes of the MAPK signaling pathway (G) but barely affects the expression level of WNT target genes (H). Data are shown as the mean ± SEM (n = 3). *p < 0.05, **p < 0.01, ***p < 0.001, t test.

(I and J) Western blot (n = 3) showing higher levels of ERK1/2 phosphorylation in shLincU mESCs (I) and $LincU^{-/-}$ mESCs (J) cultured in LIF + FBS medium.

(K) Western blot (n = 3) showing that LincU overexpression decreases the level of ERK1/2 phosphorylation when cultured in LIF + FBS medium.

(L and M) LincU knockdown-induced increases in the expression of primed-state-related genes and developmental genes are significantly compromised by MAPK/ERK inhibitor (PD0325901) treatment, as shown by qPCR (L) and western blot (M) analysis. Data are shown as the mean ± SEM (n = 3). *p < 0.05, **p < 0.01, ***p < 0.001, $^{\#}$p < 0.05, $^{\#\#}$p < 0.01, $^{\#\#\#}$p < 0.001, t test.

in most biological processes (Bononi et al., 2011). The negative correlation between LincU expression and the level of ERK1/2 phosphorylation indicates that LincU modifies ERK1/2 phosphorylation in mESCs. ERK1/2 are serine/threonine kinases that are mainly involved in signal transduction of the Ras-Raf-MEK-ERK cascade. MEK1/2 are well-known kinases that catalyze the phosphorylation of ERK1/2, whereas DUSP9 specifically hydrolyzes the phosphate group on ERK1/2 in mESCs (Figure 3A). We thus examined the protein levels of phosphorylated MEK1/2 and DUSP9 in LincU-deficient and LincU-overexpressing mESCs. Notably, no significant change in the phosphorylated MEK1/2 protein level was observed after either LincU deficiency or overexpression, whereas the protein level of DUSP9 was obviously decreased after LincU deficiency and increased with LincU overexpression (Figures 3B–3D and S4A–S4C). *In vivo* results also showed that LincU knockout decreased DUSP9 protein levels while LincU overexpression increased DUSP9 protein levels in teratomas (Figures S4D–S4G). Interestingly, the mRNA level of *Dusp9* remained unchanged after either LincU deficiency or overexpression (Figures 3E–3G), indicating that LincU might increase *Dusp9* protein stability at the post-translational level.

Considering that LincU is primarily resident in the cytoplasm, we suspected that LincU could bind to DUSP9 to increase its protein stability. To this end, a native RNA immunoprecipitation (RIP) assay was performed using a specific antibody against DUSP9 in mESCs. After pulling down DUSP9, substantial amounts of LincU were observed in the immunocomplexes (Figure 3H). Moreover, we performed the crosslinked RIP assay with a specific DUSP9 antibody, and our results further showed that LincU indeed interacted with DUSP9 (Figure S4H). To further confirm that LincU is required for the stabilization of DUSP9 protein, we treated shCtrl and shLincU mESCs with cycloheximide to disrupt the translation processes and found that the DUSP9 protein level decreased much more dramatically in LincU-deficient mESCs than in control mESCs (Figures 3I and S4I). Moreover, pretreatment with a potent proteasome inhibitor, MG132, stabilized DUSP9 protein expression in LincU-deficient mESCs, indicating that the ubiquitination-proteasome pathway is involved in LincU deficiency-induced DUSP9 degradation (Figures 3J and S4J). Immunoprecipitation using a specific DUSP9 antibody was performed after pretreatment with MG132 and blotted with an antibody against ubiquitin. Our results clearly showed polyubiquitinated DUSP9 bands, suggesting that LincU knockdown causes DUSP9 ubiquitination (Figures 3K and S4K). Collectively, these results demonstrated that LincU protects DUSP9 protein from ubiquitination-proteasome-mediated degradation in mESCs.

Dusp9 Lies Downstream of LincU to Preserve the Naïve Pluripotency of mESCs

To certify that *Dusp9* lies downstream of LincU to maintain the naïve state of mESCs, we designed a potent shRNA targeting the CDS (coding sequence) region of *Dusp9* mRNA to knock down *Dusp9* in LincU-overexpressing mESCs. The knockdown efficiency was verified by qPCR and western blot (Figures 4A, 4B, and S5A). In addition, we found that both the decreased levels of ERK1/2 phosphorylation and the decreased expression levels of primed-state-related genes triggered by LincU overexpression were significantly compromised by *Dusp9* knockdown (Figures 4A, 4B, and S5B). Moreover, the LincU-inhibited expression of DNMT3B was rescued by *Dusp9* knockdown (Figures 4C and S5C). Additionally, LincU-overexpressing mESCs recuperated their ability to transition to the primed state when *Dusp9* was downregulated (Figures 4D–4F). Taken together, our data demonstrated that *Dusp9* lies downstream of LincU to preserve the naïve pluripotency of mESCs.

LincU Is the Direct Target of NANOG in Naïve-State mESCs

Chromatin immunoprecipitation sequencing (ChIP-seq) data for ESCs from CODEX (http://codex.stemcells.cam.ac.uk/) indicated that the core transcription factors NANOG, SOX2, ESRRB, KLF4, and SMAD1 do bind to the promoter of LincU (Sanchez-Castillo et al., 2015). Thus, we tested the LincU-promoter luciferase reporter with *Sox2*, *Esrrb*, *Klf4*, and *Smad1* as well as *Nanog*. Our results showed that NANOG induced a stronger activation of LincU promoter than KLF4 and SMAD1, while SOX2 and ESRRB showed no significant activation of LincU promoter (Figure S5D). Next, we deleted two possible *Nanog*-binding motifs in LincU promoter (mutant LincU promoter) and found that reporter activity was reduced (Figure 5A). These results indicated that *Nanog* is one important upstream regulator of LincU, and these other transcription factors might regulate LincU together with NANOG. Furthermore, ChIP-PCR assay using a specific antibody against NANOG confirmed that NANOG directly binds to the promoter of LincU in naïve-state mESCs (Figure 5B).

To further confirm that LincU is downstream of *Nanog*, we performed knockdown of *Nanog* and observed a dramatic decrease of LincU transcription after *Nanog* knockdown (Figures 5C and 5D). Consistent with the results obtained from LincU knockdown, *Nanog* knockdown upregulated primed-state-related genes (Figure 5D), decreased DUSP9 protein expression and increased ERK1/2 phosphorylation (Figures 5E and S5E). Notably, *Nanog* knockdown-accelerated primed-state transition, which was characterized by a flat morphology and high expression levels of primed-state-related genes, was significantly compromised by

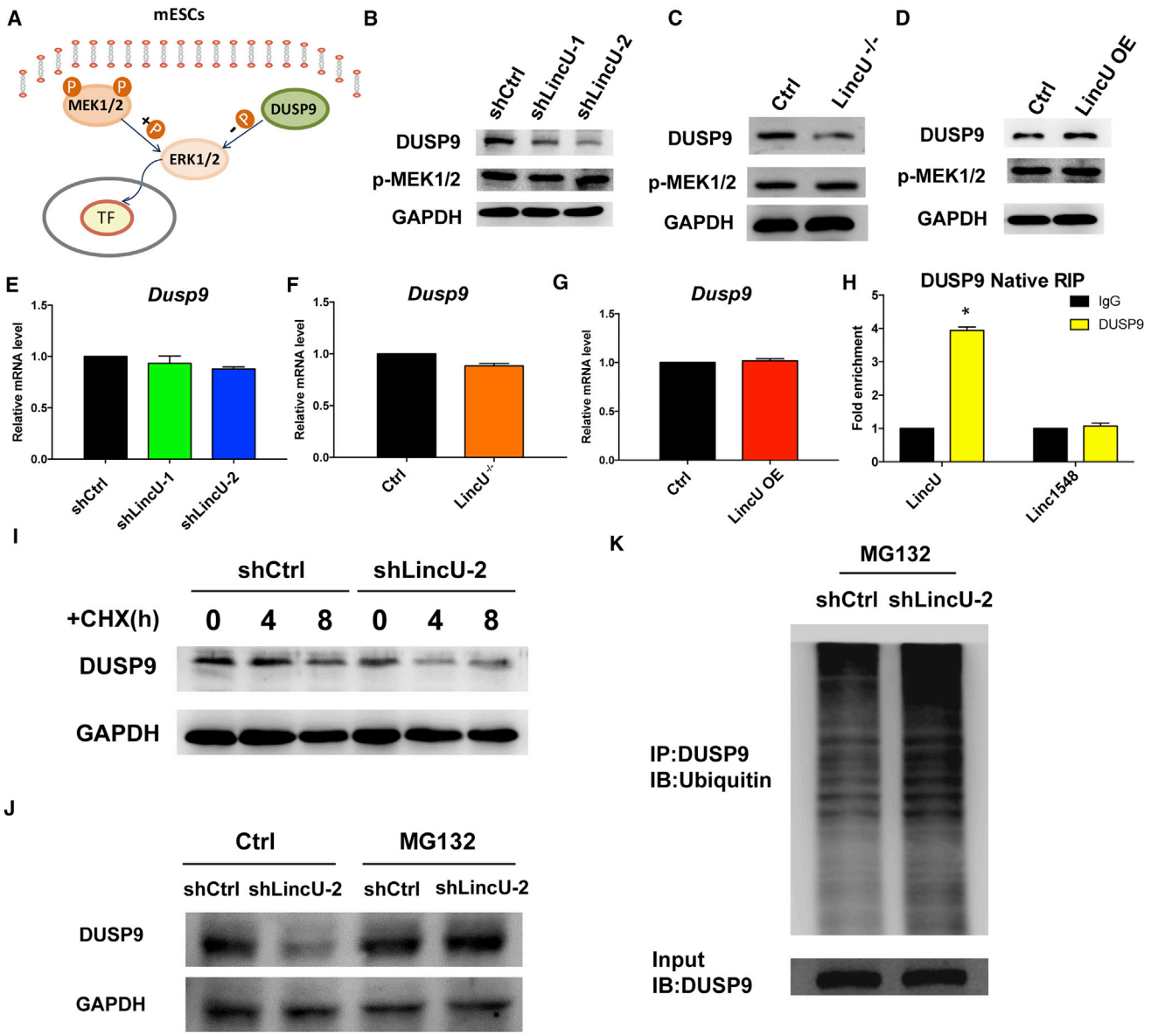

Figure 3. LincU Stabilizes the ERK-Specific Phosphatase DUSP9 in mESCs

(A) Model illustrating the phosphorylation and dephosphorylation roles of MEK1/2 and DUSP9, respectively, in the regulation of ERK1/2 phosphorylation.

(B–D) Western blot (n = 3) showing the expression level of LincU is positively correlated with the protein level of DUSP9 but not the level of MEK1/2 phosphorylation in shLincU mESCs (B), LincU$^{-/-}$ mESCs (C), and LincU-overexpressing mESCs (D).

(E–G) LincU does not change the mRNA level of *Dusp9*, as shown by qPCR analysis of shLincU mESCs (E), LincU$^{-/-}$ mESCs (F), and LincU-overexpressing mESCs (G).

(H) Native RIP assays showing the physical interaction between DUSP9 and LincU. Linc1548 acts as a negative control. Data are shown as the mean ± SEM (n = 3). *p < 0.05, t test.

(I) DUSP9 protein degradation is accelerated in shLincU mESCs compared with shCtrl mESCs after CHX (20 μg/mL) treatment.

(J) DUSP9 protein degradation in shLincU mESCs is rescued by proteasome inhibitor (MG132) treatment.

(K) LincU knockdown induces robust DUSP9 ubiquitination.

ectopic LincU expression (Figures 5F and 5G). Meanwhile, the decreased DUSP9 protein expression and increased level of ERK1/2 phosphorylation triggered by *Nanog* knockdown were also rescued by LincU overexpression (Figures 5H and S5F). Together, these data verified that LincU is the direct target of *Nanog* in naïve mESCs.

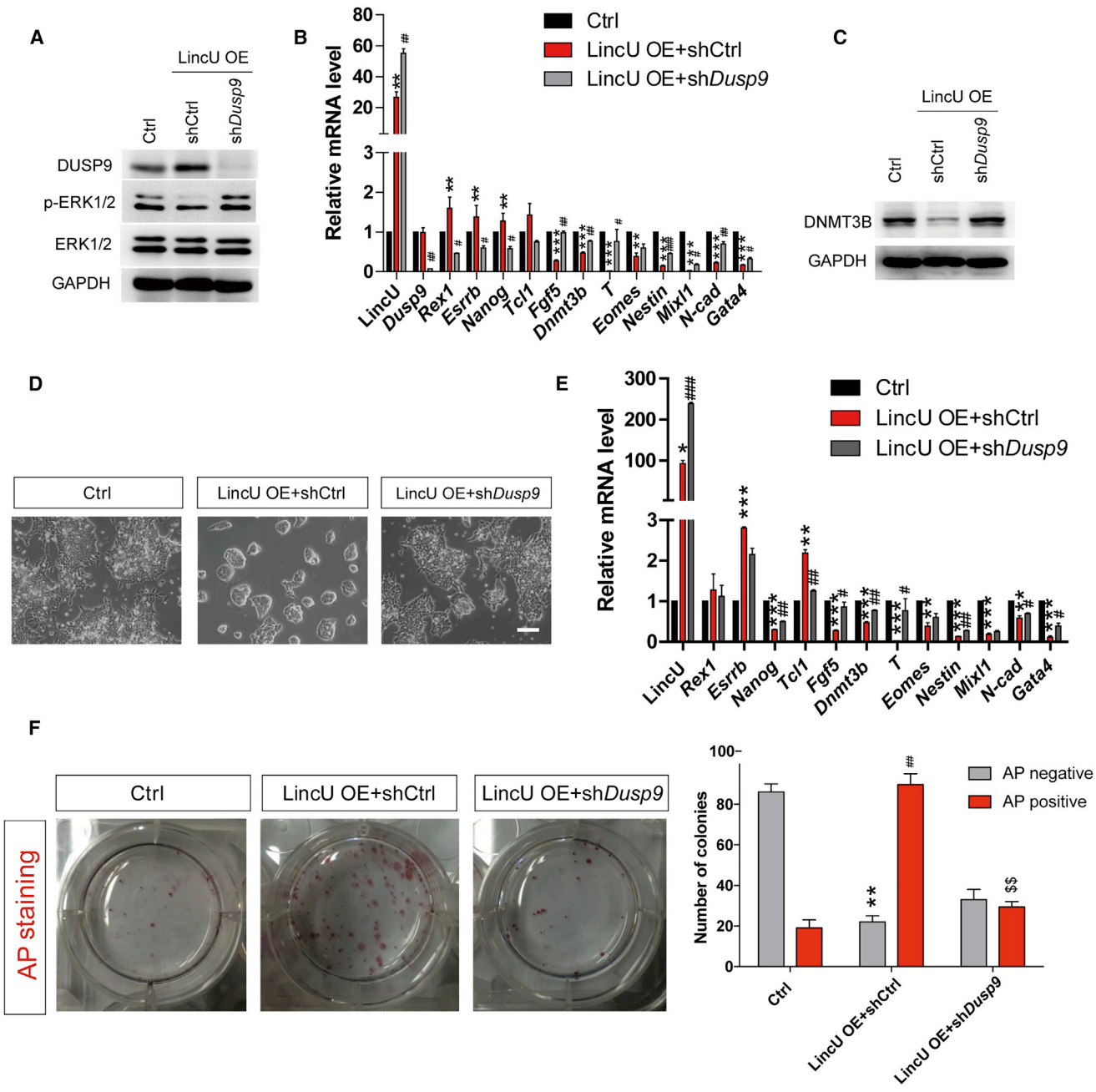

Figure 4. Dusp9 Lies Downstream of LincU to Preserve the Naïve Pluripotency of mESCs

(A) Western blot (n = 3) showing *Dusp9* knockdown rescues the LincU overexpression-induced decrease in ERK1/2 phosphorylation.

(B and C) LincU overexpression-induced inhibition of primed-state-related and developmental gene expression is significantly compromised by *Dusp9* knockdown, as shown by qPCR (B) and western blot (C) analysis in mESCs. Data are shown as the mean ± SEM (n = 3). $^{**}p < 0.01$, $^{***}p < 0.001$, $^{\#}p < 0.05$, $^{\#\#}p < 0.01$, $^{\#\#\#}p < 0.001$, t test.

(D and E) *Dusp9* knockdown restores the capacity of LincU-overexpressing mESCs to undergo epiblast induction, as shown by microscopy (D) and qPCR (E) analysis of day-2 induced epiblast cells. Data are shown as the mean ± SEM (n = 3). $^{*}p < 0.05$, $^{**}p < 0.01$, $^{***}p < 0.001$, $^{\#}p < 0.05$, $^{\#\#}p < 0.01$, $^{\#\#\#}p < 0.001$, t test. Scale bar, 100 μm.

(F) Colony-formation assay of single cells from Ctrl group and LincU-overexpression group along with shCtrl and sh*Dusp9*, respectively, 48 hr post epiblast induction. Colonies were stained for AP activity on day 6 of culture in LIF + FBS medium and deemed as either AP-positive or AP-negative. Data are shown as the mean ± SEM (n = 3). $^{**}p < 0.01$, $^{\#\#}p < 0.01$, $^{\$\$}p < 0.01$, t test.

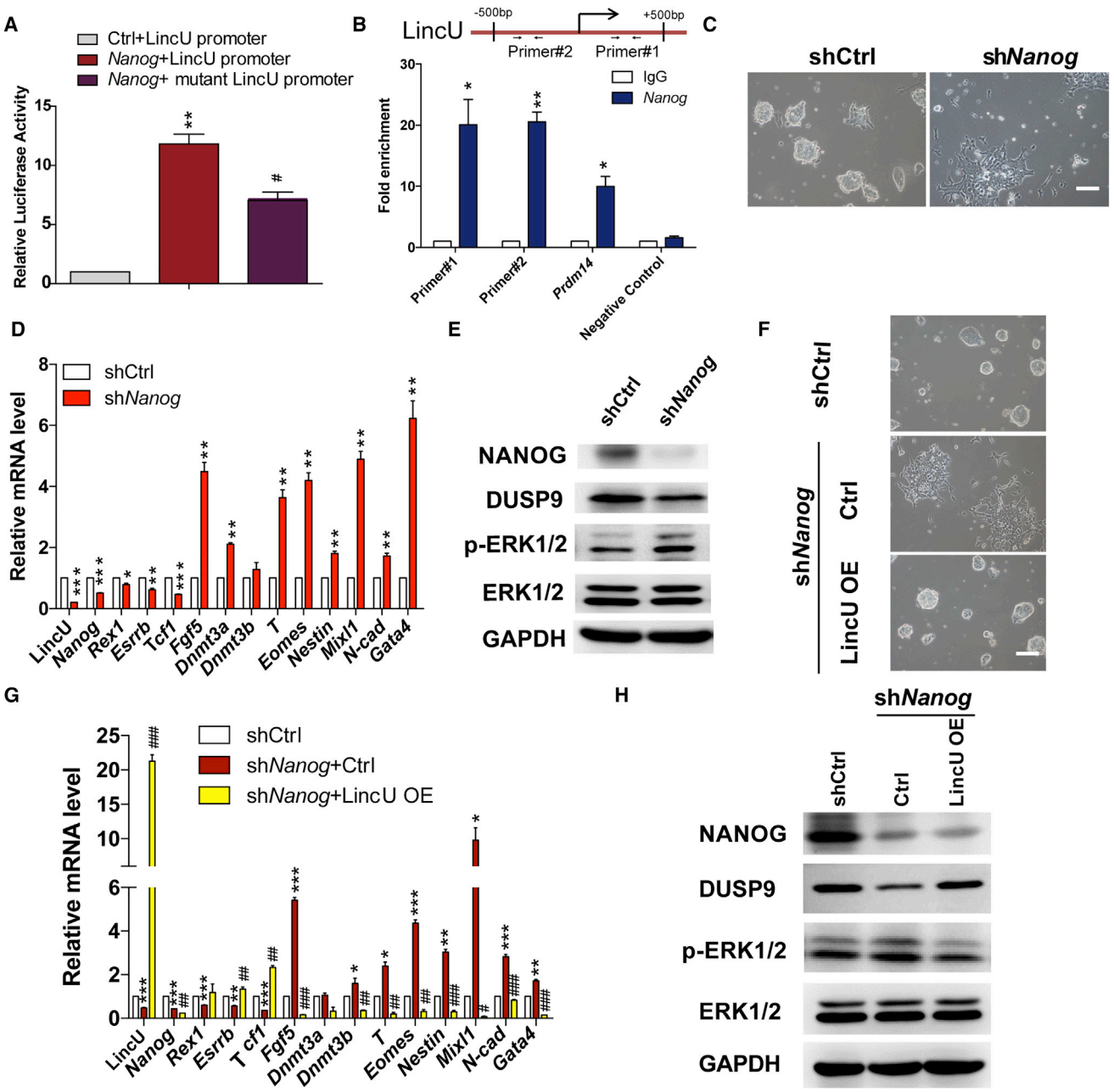

Figure 5. LincU Is the Direct Target of NANOG in Naïve-State mESCs

(A and B) NANOG directly binds to the promoter region of LincU, as shown by the luciferase reporter assay (A) and ChIP-qPCR with anti-NANOG antibody (B). *Prdm*14 acts as a positive control. The negative control amplifies an intergenic region. Data are shown as the mean ± SEM (n = 3). *p < 0.05, **p < 0.01, $^{\#}$p < 0.05, t test.

(C and D) *Nanog* knockdown induces obvious differentiation of mESCs, as shown by microscopy (C) and qPCR (D) analysis 48 hr post sh*Nanog* lentivirus infection. Data are shown as the mean ± SEM (n = 3). *p < 0.05, **p < 0.01, ***p < 0.001, t test. Scale bar, 100 μm.

(E) Western blot (n = 3) showing *Nanog* knockdown clearly decreases the protein level of DUSP9 and elevates the level of ERK1/2 phosphorylation.

(F and G) Overexpressing LincU markedly blocks the differentiation of mESCs triggered by *Nanog* knockdown, as shown by microscopy (F) and qPCR analysis (G). Data are shown as the mean ± SEM (n = 3). *p < 0.05, **p < 0.01, ***p < 0.001, $^{\#}$p < 0.5, $^{\#\#}$p < 0.01, $^{\#\#\#}$p < 0.001, t test. Scale bar, 100 μm.

(H) Western blot (n = 3) showing the decreased protein level of DUSP9 and elevated level of ERK1/2 phosphorylation in sh*Nanog* mESCs are significantly compromised by LincU overexpression.

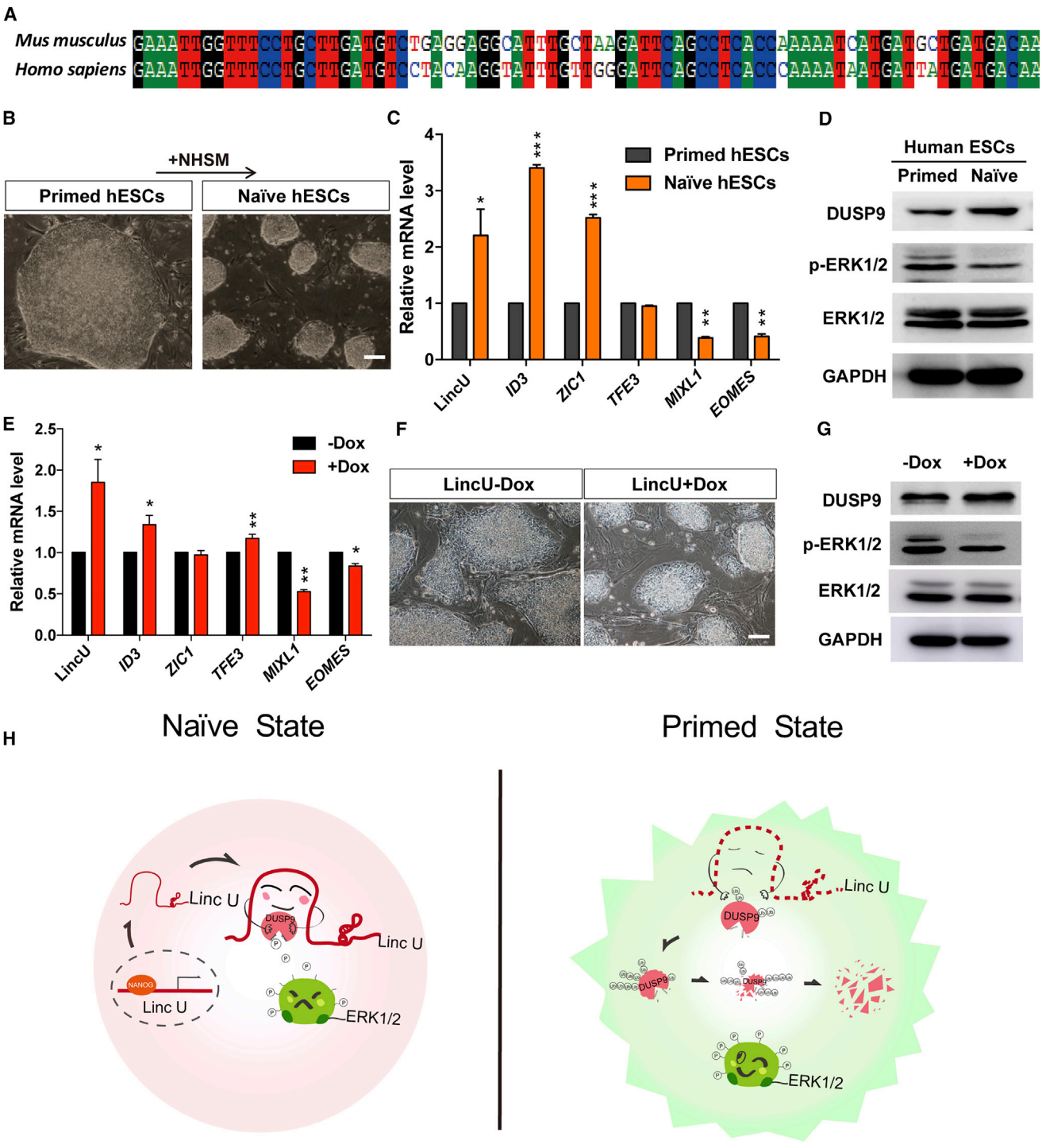

Figure 6. Functional Role of LincU Is Conserved in hESCs

(A) The matched sequence of mouse LincU in the human genome indicates that LincU is conserved in humans.

(B) Morphology of primed hESCs and naïve hESCs. Scale bar, 100 μm.

(C) LincU is highly expressed in naïve hESCs compared with primed hESCs. Data are shown as the mean ± SEM (n = 3). *p < 0.05, **p < 0.01, ***p < 0.001, t test.

(D) Western blot (n = 3) showing higher protein levels of DUSP9 and lower levels of ERK1/2 phosphorylation are detected in naïve hESCs than in primed hESCs.

(legend continued on next page)

The Functional Role of LincU Is Conserved in hESCs

Naïve-state hESCs show great promise for clinical cellular supplementation therapy (Batista and Chang, 2013). In addition, lincRNAs commonly exhibit high mutation frequencies and are rarely conserved from rodents to humans. Thus, conserved and functional lincRNAs involved in the transition between naïve and primed hESCs are rarely reported. Fortunately, mouse LincU shares a homology region with human genome (Figure 6A), indicating that LincU is an evolutionarily conserved lincRNA. We thus designed a specific pair of primers for the qPCR amplification of human LincU and examined the relative expression levels between naïve and primed hESCs (Figure 6B). The results showed that the expression of LincU was higher in naïve-state hESCs than that in primed-state hESCs, which is similar to the expression patterns of reported human naïve-state-specific genes (Gafni et al., 2013) (Figure 6C). Importantly, DUSP9 protein expression levels were higher and ERK1/2 phosphorylation levels were lower in naïve hESCs than in primed-state hESCs (Figures 6D and S6A), indicating the conserved role of LincU in stabilizing the DUSP9 protein.

Moreover, ectopic expression of human LincU in hESCs successfully induced hESCs to a naïve-like state under NHSM (naïve human stem cell medium) without an MAPK signaling pathway inhibitor, as characterized by a more domed morphology, high expression levels of naïve-state-related genes, and lower expression levels of primed-state-related genes (Figures 6E and 6F). Notably, human LincU overexpression in hESCs also protected DUSP9 from degradation to a greater extent and inhibited the phosphorylation of ERK1/2 (Figures 6G and S6B). Taken together, our findings uncovered an evolutionarily conserved naïve-state-associated lincRNA named LincU that plays a pivotal role in maintaining the naïve state of both mouse and human ESCs. *Nanog*-induced LincU directly binds and stabilizes DUSP9 protein, which then constitutively inhibits the ERK1/2 signaling pathway, critically contributing to the maintenance of the naïve state (Figure 6H).

DISCUSSION

Until recently the functional roles of lncRNAs, which were once underestimated and regarded as "junk" in the genome, have been revealed in multiple biological processes, including early embryonic development and adult aging (Balakirev and Ayala, 2003; Grote et al., 2013; Lee and Bartolomei, 2013; Ulitsky et al., 2011; Zhang et al., 2012). Although an increasing number of lncRNAs that participate in controlling the pluripotency of mESCs have been discovered (Guttman et al., 2011), identification of functional lncRNAs involved in maintaining the naïve state of mESCs, which are closer to early-stage embryos and have higher pluripotency, is still missing. Here, we found that LincU is specifically and highly expressed in naïve mESCs and that its expression decreases dramatically as mESCs exit the naïve state. Moreover, we verified that LincU is both indispensable and sufficient to maintain the naïve state of mESCs with both *in vivo* and *in vitro* assays, similar to those well-defined naïve-state-associated transcription factors, such as *Klf2*, *Klf4*, *Esrrb*, and *Nanog*. Therefore, our research identified a vital naïve-state-associated lincRNA that is involved in maintaining the naïve state.

Early embryonic development is a complicated and elaborate process that is precisely controlled by extrinsic signaling transduction and intrinsic epigenetic and transcriptional regulation. In addition, extrinsic signaling pathways are consistently acknowledged as the main force underlying early lineage commitment (Kalkan and Smith, 2014). Among those pathways, MAPK/ERK signaling has been identified as a pivotal signaling pathway involved in early embryonic development both *in vivo* and *in vitro*, playing roles in gastrulation, transition from the naïve to the primed state, stabilization of primed-state pluripotent stem cells, and early neural lineage commitment (Kunath et al., 2007; Nichols et al., 2009; Nichols and Smith, 2009). However, the intrinsic factor that tactically modulates the activity of MAPK/ERK signaling remains unelucidated. In the present study, we identified LincU as an intrinsic inhibitor of the MAPK/ERK signaling pathway in naïve-state mESCs. Notably, we revealed that LincU stabilizes the DUSP9 protein, a BMP4/SMADs-induced and mESC-specific ERK1/2 phosphatase, by interacting with DUSP9 and preventing its ubiquitination/degradation cascade (Li et al., 2012). Although the details regarding the protective effects of LincU on DUSP9 must be further explored, the present study clearly demonstrates that intrinsic inhibition of the MAPK/ERK signaling pathway by the LincU/DUSP9 axis is indispensable for the maintenance of the naïve state.

(E and F) LincU overexpression leads to naïve-state-like hESCs when cultured in NHSM without PD0325901, as shown by qPCR (E) and microscopy (F). Data are shown as the mean ± SEM (n = 3). *p < 0.05, **p < 0.01, t test. Scale bar, 100 μm.

(G) Western blot (n = 3) showing that overexpressing LincU increases the protein level of DUSP9 and decreases the level of ERK1/2 phosphorylation.

(H) Model showing that *Nanog*-activated LincU directly binds and stabilizes the ERK-specific phosphatase DUSP9 and then inhibits MAPK/ERK signaling activity to maintain the naïve pluripotent state of ESCs.

When cultured in medium supplemented with LIF and serum, mESCs are a hodgepodge of both naïve and primed mESCs, which are well defined by the expression level of *Nanog* (Festuccia et al., 2012). *Nanog* has been reported to be the gateway to naïve pluripotency, and forced *Nanog* expression is sufficient to drive the cytokine-independent self-renewal of naïve-state mESCs (Chambers et al., 2007). Interestingly, inhibition of the MAPK/ERK signaling pathway leads to effects similar to those of *Nanog* overexpression. However, the relationship between *Nanog* and MAPK/ERK signaling in naïve-state mESCs remains to be elucidated. In the present study, we verified a negative correlation between *Nanog* expression and the activity of MAPK/ERK signaling. In addition, we demonstrated that *Nanog* directly activates the expression of LincU, which further stabilizes DUSP9 protein expression and results in inhibition of the MAPK/ERK signaling pathway in naïve-state mESCs. Importantly, we found that forced expression of LincU can inhibit the MAPK/ERK signaling pathway and drive the self-renewal of *Nanog*-deficient mESCs. Collectively, our study clearly revealed that the intrinsic transcription factor *Nanog* inhibits MAPK/ERK signaling pathway activity by directly inducing the transcription of LincU in naïve-state mESCs.

Species differences in early embryonic development, especially the stage around implantation, cause the results acquired from animal models to be suboptimal for human applications. Most famously, signaling pathways implicated in the maintenance of mESCs involve activation of the LIF/STAT3 and BMP signaling pathways or inhibition of the FGF/ERK and GSK3β signaling pathways, whereas the self-renewal of hESCs requires activation of the bFGF/ERK and activin/nodal signaling pathways (James et al., 2005; Li et al., 2007). Recently, numerous studies have identified a combination of five kinase inhibitors, including an ERK1/2 inhibitor together with LIF and activin A (5i/L/A), that enables the conversion of pre-existing hESCs to the naïve state, indicating the conserved role of MAPK/ERK signaling in the maintenance of naïve-state hESCs (Gafni et al., 2013). Here, we demonstrated that LincU is conserved and more highly expressed in naïve-state hESCs, along with higher protein level of DUSP9 and lower MAPK/ERK signaling activity in naïve-state hESCs compared with those in primed-state hESCs. Notably, we recapitulated the functional interplay between LincU and DUSP9 in hESCs, and the results coincided exactly with those in mice.

In summary, we report an evolutionarily conserved naïve-state-associated lincRNA, LincU, which plays a pivotal role in maintaining the naïve state of both mouse and human ESCs. *Nanog*-induced LincU directly binds and stabilizes the DUSP9 protein and then constitutively inhibits the ERK1/2 signaling pathway, which critically contributes to maintenance of the naïve state. Collectively, our data shed light on a crucial role of the intrinsic *Nanog*/LincU/DUSP9/ERK signaling pathway in naïve-state maintenance, which is potentially beneficial for capturing the highest value of naïve-state ESCs in future research and therapeutic applications.

EXPERIMENTAL PROCEDURES

Animal Studies

All experiments involving animals were approved by the Institutional Animal Care and Use Committee of Tongji University under the Guide for the Care and Use of Laboratory Animals (NIH Guide).

Induction of Epiblast-like Cells

A 6-well plate was coated with 0.1% (w/v) gelatin (Gibco) overnight, and mESCs were trypsinized and plated (3×10^5) into each well in N2B27-based medium containing 1% knockout serum replacement medium (Gibco), 12 ng/mL bFGF (Sino Biological), and 20 ng/mL activin A (R&D Systems).

Colony-Formation Assay

Colony-formation assay was performed as previously described (Karwacki-Neisius et al., 2013). In total, 600 cells were plated into each well of a 6-well plate and cultured in mESC medium for 6 days. The colonies were then fixed with 4% paraformaldehyde in PBS for 1 min at room temperature, and AP staining was performed using an Alkaline Phosphatase Kit (Sigma) for 20 min at 37°C. The AP-positive and -negative colony numbers were calculated.

Statistical Analysis

All statistical data are presented as the mean ± SEM of at least three independent experiments. Statistical significance was determined using unpaired two-tailed Student's t tests (in figures $^{*}p < 0.05$, $^{**}p < 0.01$, $^{***}p < 0.001$, $^{\#}p < 0.05$, $^{\#\#}p < 0.01$, $^{\#\#}p < 0.001$, $^{\$}p < 0.05$, $^{\$\$}p < 0.01$, $^{\$\$\$}p < 0.001$).

ACCESSION NUMBERS

The NCBI GEO accession number for the microarray data reported in this paper is GEO: GSE107418.

SUPPLEMENTAL INFORMATION

Supplemental Information includes Supplemental Experimental Procedures, six figures, and one table and can be found with this article online at https://doi.org/10.1016/j.stemcr.2018.06.010.

AUTHOR CONTRIBUTIONS

Z.J. and G.L. contributed equally to this work, including study conception and design, performing the experiments, data analysis, and manuscript writing. D.Y., M.B., J.L., D.S., Y.Y., and F.Z. were involved in manuscript preparation. Y.D. contributed to the microarray data analysis. W.J., W.C., X.G., G.W., and X.W. contributed to the study design and supervised the project. J.K. designed and

supervised the project and provided financial support and manuscript writing.

ACKNOWLEDGMENTS

This work was supported by grants obtained from the Ministry of Science and Technology (grant number 2016YFA0101300), the National Natural Science Foundation of China (grant numbers 81530042, 31721003, 31571529, 31571519, 31471250, 31701110, 31571390, 31771506, 81600675, and 31671533), Ministry of Education grant IRT_15R51, Science and Technology Commission of Shanghai Municipality (grant number 15JC1403201), the Fundamental Research Funds for the Central Universities (1500219106, 20002310002, 1515219039, and 1515219040), and Shanghai Municipal Medical and Health Discipline Construction projects (grant number 2017ZZ02015).

Received: January 12, 2018
Revised: June 15, 2018
Accepted: June 15, 2018
Published: July 12, 2018

REFERENCES

Balakirev, E.S., and Ayala, F.J. (2003). Pseudogenes: are they "junk" or functional DNA? Annu. Rev. Genet. *37*, 123–151.

Batista, P.J., and Chang, H.Y. (2013). Long noncoding RNAs: cellular address codes in development and disease. Cell *152*, 1298–1307.

Bononi, A., Agnoletto, C., De Marchi, E., Marchi, S., Patergnani, S., Bonora, M., Giorgi, C., Missiroli, S., Poletti, F., Rimessi, A., et al. (2011). Protein kinases and phosphatases in the control of cell fate. Enzyme Res. *2011*, 329098.

Borgel, J., Guibert, S., Li, Y., Chiba, H., Schubeler, D., Sasaki, H., Forne, T., and Weber, M. (2010). Targets and dynamics of promoter DNA methylation during early mouse development. Nat. Genet. *42*, 1093–1100.

Bradley, A., Evans, M., Kaufman, M.H., and Robertson, E. (1984). Formation of germ-line chimaeras from embryo-derived teratocarcinoma cell lines. Nature *309*, 255–256.

Brons, I.G., Smithers, L.E., Trotter, M.W., Rugg-Gunn, P., Sun, B., Chuva de Sousa Lopes, S.M., Howlett, S.K., Clarkson, A., Ahrlund-Richter, L., Pedersen, R.A., et al. (2007). Derivation of pluripotent epiblast stem cells from mammalian embryos. Nature *448*, 191–195.

Chambers, I., Colby, D., Robertson, M., Nichols, J., Lee, S., Tweedie, S., and Smith, A. (2003). Functional expression cloning of Nanog, a pluripotency sustaining factor in embryonic stem cells. Cell *113*, 643–655.

Chambers, I., Silva, J., Colby, D., Nichols, J., Nijmeijer, B., Robertson, M., Vrana, J., Jones, K., Grotewold, L., and Smith, A. (2007). Nanog safeguards pluripotency and mediates germline development. Nature *450*, 1230–1234.

Dinger, M.E., Amaral, P.P., Mercer, T.R., Pang, K.C., Bruce, S.J., Gardiner, B.B., Askarian-Amiri, M.E., Ru, K., Solda, G., Simons, C., et al. (2008). Long noncoding RNAs in mouse embryonic stem cell pluripotency and differentiation. Genome Res. *18*, 1433–1445.

Dunn, S.J., Martello, G., Yordanov, B., Emmott, S., and Smith, A.G. (2014). Defining an essential transcription factor program for naive pluripotency. Science *344*, 1156–1160.

Evans, M.J., and Kaufman, M.H. (1981). Establishment in culture of pluripotential cells from mouse embryos. Nature *292*, 154–156.

Fatica, A., and Bozzoni, I. (2014). Long non-coding RNAs: new players in cell differentiation and development. Nat. Rev. Genet. *15*, 7–21.

Festuccia, N., Osorno, R., Halbritter, F., Karwacki-Neisius, V., Navarro, P., Colby, D., Wong, F., Yates, A., Tomlinson, S.R., and Chambers, I. (2012). Esrrb is a direct Nanog target gene that can substitute for Nanog function in pluripotent cells. Cell Stem Cell *11*, 477–490.

Gafni, O., Weinberger, L., Mansour, A.A., Manor, Y.S., Chomsky, E., Ben-Yosef, D., Kalma, Y., Viukov, S., Maza, I., Zviran, A., et al. (2013). Derivation of novel human ground state naive pluripotent stem cells. Nature *504*, 282–286.

Greber, B., Wu, G., Bernemann, C., Joo, J.Y., Han, D.W., Ko, K., Tapia, N., Sabour, D., Sterneckert, J., Tesar, P., et al. (2010). Conserved and divergent roles of FGF signaling in mouse epiblast stem cells and human embryonic stem cells. Cell Stem Cell *6*, 215–226.

Grote, P., Wittler, L., Hendrix, D., Koch, F., Wahrisch, S., Beisaw, A., Macura, K., Blass, G., Kellis, M., Werber, M., et al. (2013). The tissue-specific lncRNA Fendrr is an essential regulator of heart and body wall development in the mouse. Dev. Cell *24*, 206–214.

Guttman, M., Donaghey, J., Carey, B.W., Garber, M., Grenier, J.K., Munson, G., Young, G., Lucas, A.B., Ach, R., Bruhn, L., et al. (2011). lincRNAs act in the circuitry controlling pluripotency and differentiation. Nature *477*, 295–300.

Guttman, M., and Rinn, J.L. (2012). Modular regulatory principles of large non-coding RNAs. Nature *482*, 339–346.

Hackett, J.A., and Surani, M.A. (2014). Regulatory principles of pluripotency: from the ground state up. Cell Stem Cell *15*, 416–430.

Hayashi, K., Ohta, H., Kurimoto, K., Aramaki, S., and Saitou, M. (2011). Reconstitution of the mouse germ cell specification pathway in culture by pluripotent stem cells. Cell *146*, 519–532.

James, D., Levine, A.J., Besser, D., and Hemmati-Brivanlou, A. (2005). TGFbeta/activin/nodal signaling is necessary for the maintenance of pluripotency in human embryonic stem cells. Development *132*, 1273–1282.

Kalkan, T., and Smith, A. (2014). Mapping the route from naive pluripotency to lineage specification. Philos. Trans. R. Soc. Lond. B Biol. Sci. *369*. https://doi.org/10.1098/rstb.2013.0540.

Karwacki-Neisius, V., Goke, J., Osorno, R., Halbritter, F., Ng, J.H., Weisse, A.Y., Wong, F.C., Gagliardi, A., Mullin, N.P., Festuccia, N., et al. (2013). Reduced Oct4 expression directs a robust pluripotent state with distinct signaling activity and increased enhancer occupancy by Oct4 and Nanog. Cell Stem Cell *12*, 531–545.

Kunath, T., Saba-El-Leil, M.K., Almousailleakh, M., Wray, J., Meloche, S., and Smith, A. (2007). FGF stimulation of the Erk1/2 signalling cascade triggers transition of pluripotent embryonic stem cells from self-renewal to lineage commitment. Development *134*, 2895–2902.

Lee, J.T., and Bartolomei, M.S. (2013). X-inactivation, imprinting, and long noncoding RNAs in health and disease. Cell *152*, 1308–1323.

Leitch, H.G., and Smith, A. (2013). The mammalian germline as a pluripotency cycle. Development *140*, 2495–2501.

Li, G., Jiapaer, Z., Weng, R., Hui, Y., Jia, W., Xi, J., Wang, G., Zhu, S., Zhang, X., Feng, D., et al. (2017). Dysregulation of the SIRT1/OCT6 Axis contributes to environmental stress-induced neural induction defects. Stem Cell Reports *8*, 1270–1286.

Li, J., Wang, G., Wang, C., Zhao, Y., Zhang, H., Tan, Z., Song, Z., Ding, M., and Deng, H. (2007). MEK/ERK signaling contributes to the maintenance of human embryonic stem cell self-renewal. Differentiation *75*, 299–307.

Li, Z., Fei, T., Zhang, J., Zhu, G., Wang, L., Lu, D., Chi, X., Teng, Y., Hou, N., Yang, X., et al. (2012). BMP4 signaling acts via dual-specificity phosphatase 9 to control ERK activity in mouse embryonic stem cells. Cell Stem Cell *10*, 171–182.

Marks, H., Kalkan, T., Menafra, R., Denissov, S., Jones, K., Hofemeister, H., Nichols, J., Kranz, A., Stewart, A.F., Smith, A., et al. (2012). The transcriptional and epigenomic foundations of ground state pluripotency. Cell *149*, 590–604.

Martin, G.R. (1981). Isolation of a pluripotent cell line from early mouse embryos cultured in medium conditioned by teratocarcinoma stem cells. Proc. Natl. Acad. Sci. USA *78*, 7634–7638.

Mitsui, K., Tokuzawa, Y., Itoh, H., Segawa, K., Murakami, M., Takahashi, K., Maruyama, M., Maeda, M., and Yamanaka, S. (2003). The homeoprotein Nanog is required for maintenance of pluripotency in mouse epiblast and ES cells. Cell *113*, 631–642.

Murakami, K., Gunesdogan, U., Zylicz, J.J., Tang, W.W.C., Sengupta, R., Kobayashi, T., Kim, S., Butler, R., Dietmann, S., and Surani, M.A. (2016). NANOG alone induces germ cells in primed epiblast in vitro by activation of enhancers. Nature *529*, 403–407.

Nagano, T., Mitchell, J.A., Sanz, L.A., Pauler, F.M., Ferguson-Smith, A.C., Feil, R., and Fraser, P. (2008). The Air noncoding RNA epigenetically silences transcription by targeting G9a to chromatin. Science *322*, 1717–1720.

Nichols, J., Chambers, I., Taga, T., and Smith, A. (2001). Physiological rationale for responsiveness of mouse embryonic stem cells to gp130 cytokines. Development *128*, 2333–2339.

Nichols, J., Silva, J., Roode, M., and Smith, A. (2009). Suppression of Erk signalling promotes ground state pluripotency in the mouse embryo. Development *136*, 3215–3222.

Nichols, J., and Smith, A. (2009). Naive and primed pluripotent states. Cell Stem Cell *4*, 487–492.

Niwa, H., Ogawa, K., Shimosato, D., and Adachi, K. (2009). A parallel circuit of LIF signalling pathways maintains pluripotency of mouse ES cells. Nature *460*, 118–122.

Ogawa, K., Saito, A., Matsui, H., Suzuki, H., Ohtsuka, S., Shimosato, D., Morishita, Y., Watabe, T., Niwa, H., and Miyazono, K. (2007). Activin-Nodal signaling is involved in propagation of mouse embryonic stem cells. J. Cell Sci. *120*, 55–65.

Pandey, R.R., Mondal, T., Mohammad, F., Enroth, S., Redrup, L., Komorowski, J., Nagano, T., Mancini-Dinardo, D., and Kanduri, C. (2008). Kcnq1ot1 antisense noncoding RNA mediates lineage-specific transcriptional silencing through chromatin-level regulation. Mol. Cell *32*, 232–246.

Rinn, J.L., and Chang, H.Y. (2012). Genome regulation by long noncoding RNAs. Annu. Rev. Biochem. *81*, 145–166.

Roskoski, R., Jr. (2012). ERK1/2 MAP kinases: structure, function, and regulation. Pharmacol. Res. *66*, 105–143.

Sanchez-Castillo, M., Ruau, D., Wilkinson, A.C., Ng, F.S., Hannah, R., Diamanti, E., Lombard, P., Wilson, N.K., and Gottgens, B. (2015). CODEX: a next-generation sequencing experiment database for the haematopoietic and embryonic stem cell communities. Nucleic Acids Res. *43*, D1117–D1123.

Stuart, H.T., van Oosten, A.L., Radzisheuskaya, A., Martello, G., Miller, A., Dietmann, S., Nichols, J., and Silva, J.C. (2014). NANOG amplifies STAT3 activation and they synergistically induce the naive pluripotent program. Curr. Biol. *24*, 340–346.

Taniue, K., Kurimoto, A., Sugimasa, H., Nasu, E., Takeda, Y., Iwasaki, K., Nagashima, T., Okada-Hatakeyama, M., Oyama, M., Kozuka-Hata, H., et al. (2016). Long noncoding RNA UPAT promotes colon tumorigenesis by inhibiting degradation of UHRF1. Proc. Natl. Acad. Sci. USA *113*, 1273–1278.

Tesar, P.J., Chenoweth, J.G., Brook, F.A., Davies, T.J., Evans, E.P., Mack, D.L., Gardner, R.L., and McKay, R.D. (2007). New cell lines from mouse epiblast share defining features with human embryonic stem cells. Nature *448*, 196–199.

Ulitsky, I., Shkumatava, A., Jan, C.H., Sive, H., and Bartel, D.P. (2011). Conserved function of lincRNAs in vertebrate embryonic development despite rapid sequence evolution. Cell *147*, 1537–1550.

Wang, P., Xue, Y., Han, Y., Lin, L., Wu, C., Xu, S., Jiang, Z., Xu, J., Liu, Q., and Cao, X. (2014). The STAT3-binding long noncoding RNA lnc-DC controls human dendritic cell differentiation. Science *344*, 310–313.

Ying, Q.L., Wray, J., Nichols, J., Batlle-Morera, L., Doble, B., Woodgett, J., Cohen, P., and Smith, A. (2008). The ground state of embryonic stem cell self-renewal. Nature *453*, 519–523.

Yoon, J.H., Abdelmohsen, K., Srikantan, S., Yang, X., Martindale, J.L., De, S., Huarte, M., Zhan, M., Becker, K.G., and Gorospe, M. (2012). LincRNA-p21 suppresses target mRNA translation. Mol. Cell *47*, 648–655.

Yoshida, K., Chambers, I., Nichols, J., Smith, A., Saito, M., Yasukawa, K., Shoyab, M., Taga, T., and Kishimoto, T. (1994). Maintenance of the pluripotential phenotype of embryonic stem cells through direct activation of gp130 signalling pathways. Mech. Dev. *45*, 163–171.

Young, R.A. (2011). Control of the embryonic stem cell state. Cell *144*, 940–954.

Zhang, B., Arun, G., Mao, Y.S., Lazar, Z., Hung, G., Bhattacharjee, G., Xiao, X., Booth, C.J., Wu, J., Zhang, C., et al. (2012). The lncRNA Malat1 is dispensable for mouse development but its transcription plays a cis-regulatory role in the adult. Cell Rep. *2*, 111–123.

Zheng, J., Huang, X., Tan, W., Yu, D., Du, Z., Chang, J., Wei, L., Han, Y., Wang, C., Che, X., et al. (2016). Pancreatic cancer risk variant in LINC00673 creates a miR-1231 binding site and interferes with PTPN11 degradation. Nat. Genet. *48*, 747–757.

Stem Cell Reports, Volume *11*

Supplemental Information

LincU Preserves Naïve Pluripotency by Restricting ERK Activity in Embryonic Stem Cells

Zeyidan Jiapaer, Guoping Li, Dan Ye, Mingliang Bai, Jianguo Li, Xudong Guo, Yanhua Du, Dingwen Su, Wenwen Jia, Wen Chen, Guiying Wang, Yangyang Yu, Fugui Zhu, Xiaoping Wan, and Jiuhong Kang

SUPPLEMENTAL FIGURES

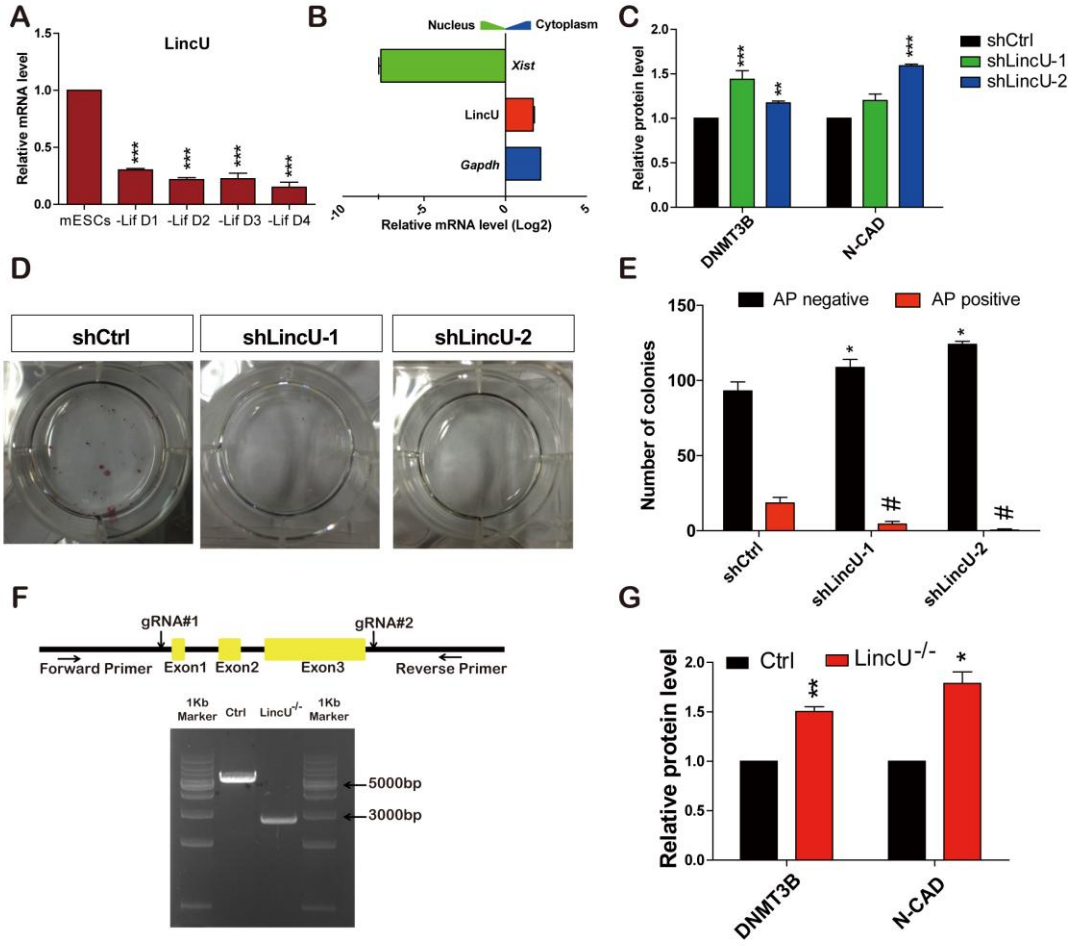

Figure S1. LincU is both essential and sufficient for maintaining the naïve pluripotency of mESCs. Related to Figure 1

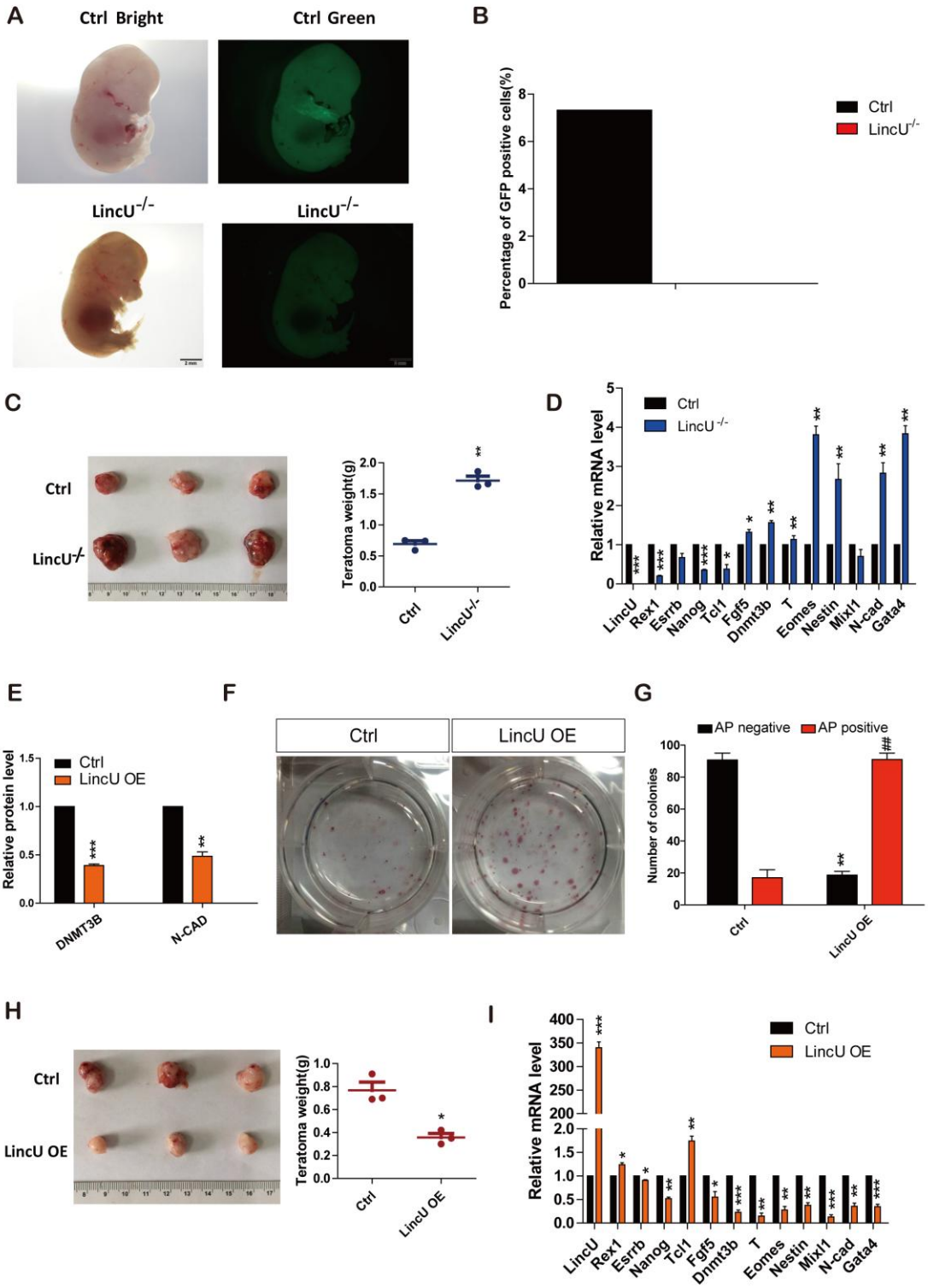

Figure S2. LincU is both essential and sufficient for maintaining the naïve pluripotency of mESCs. Related to Figure 1

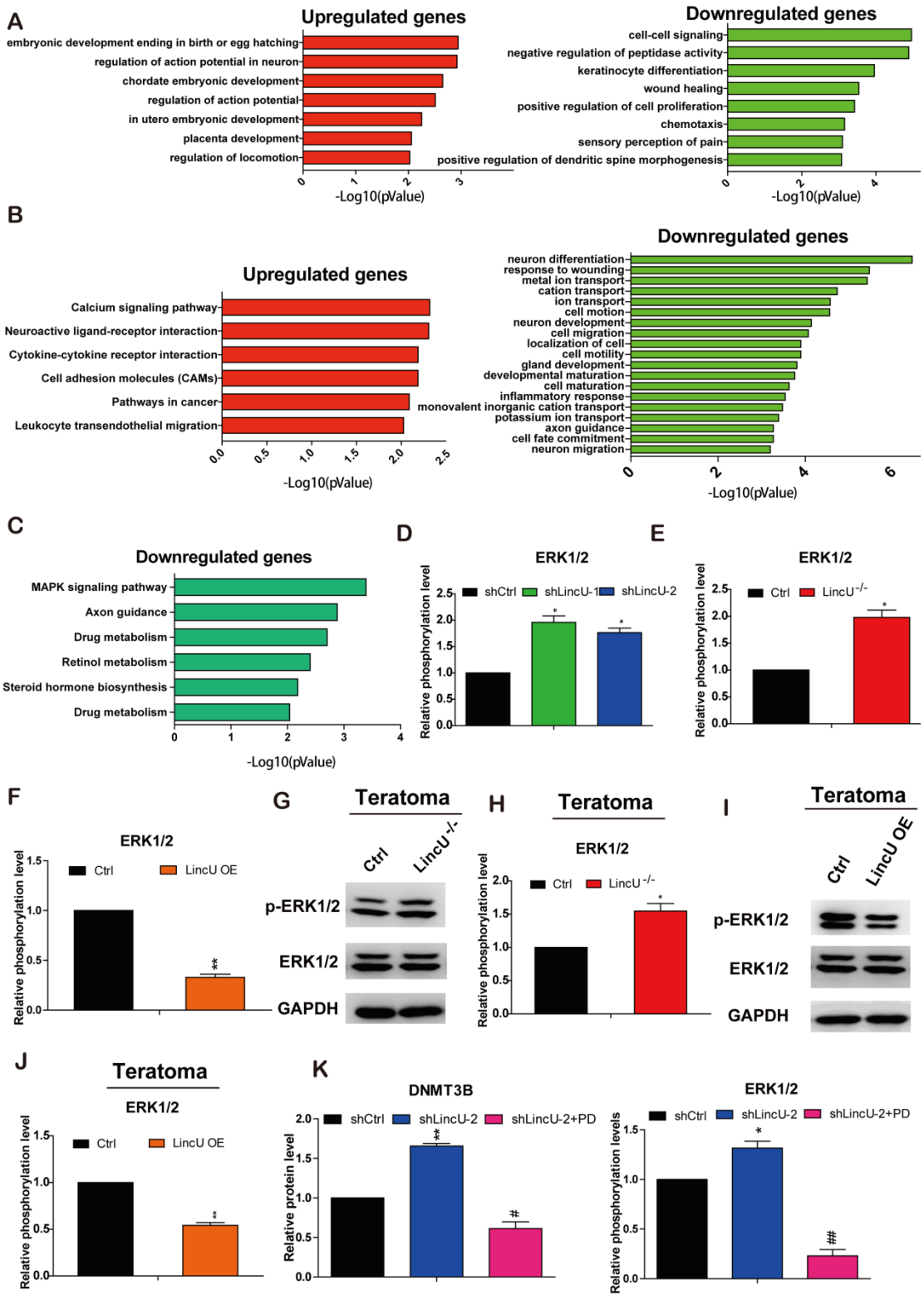

Figure S3. LincU specifically inhibits the MAPK-ERK signaling pathway. Related to Figure 2

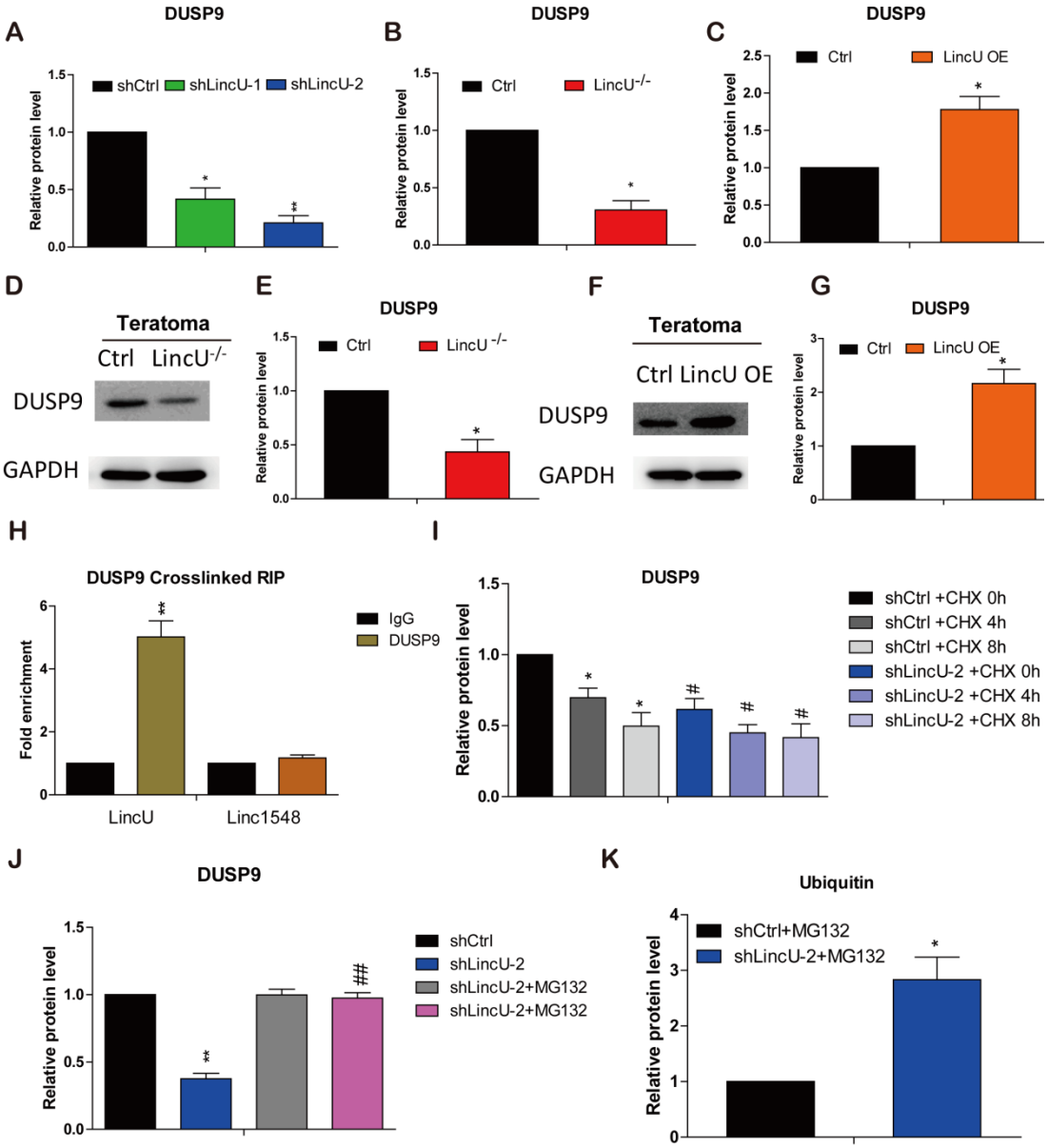

Figure S4. LincU stabilizes the ERK-specific phosphatase DUSP9 in mESCs. Related to Figure 3

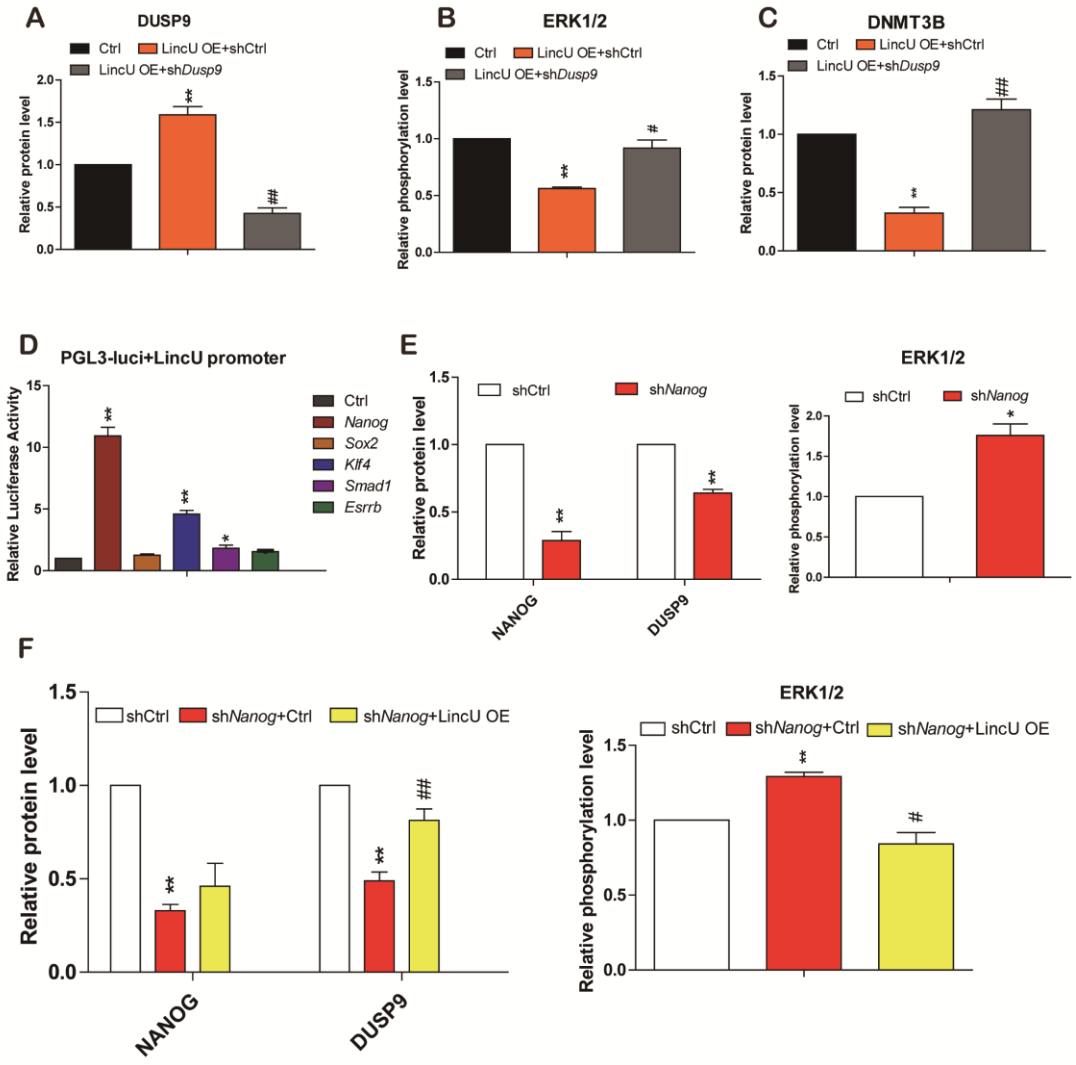

Figure S5. LincU is the direct target of NANOG in naïve-state mESCs. Related to Figure 4 and Figure 5

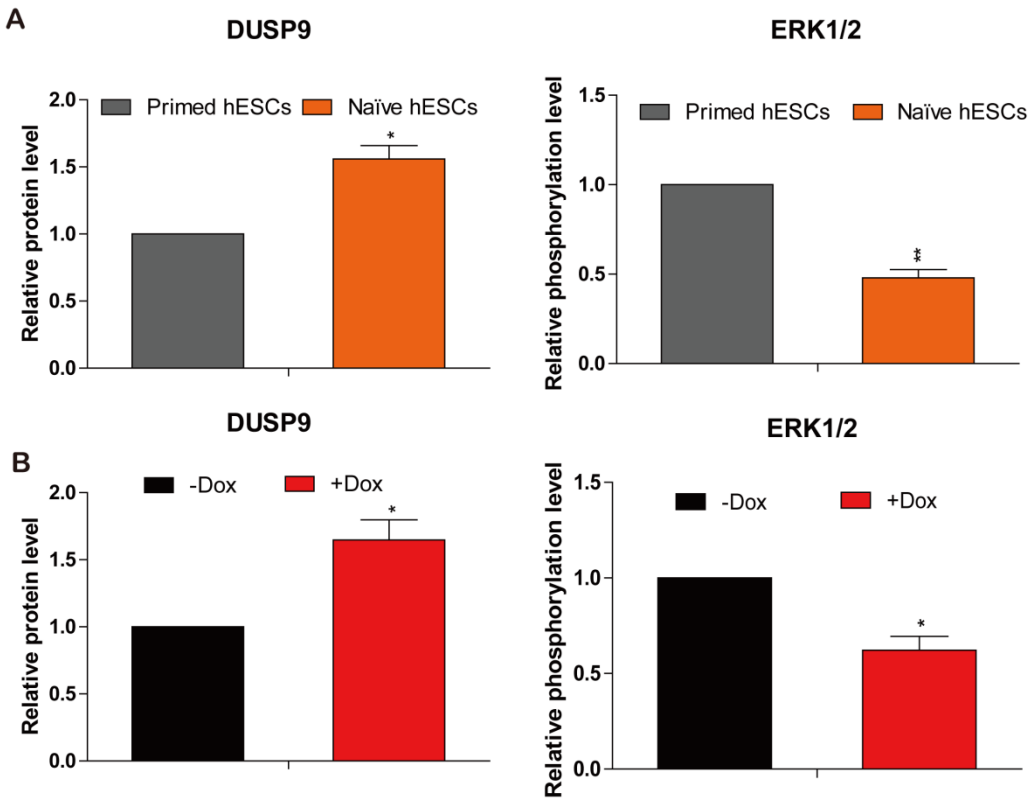

Figure S6. Functional role of LincU is conserved in hESCs. Related to Figure 6

SUPPLEMENTAL FIGURE LEGENDS

Figure S1. LincU is both essential and sufficient for maintaining the naïve pluripotency of mESCs. Related to Figure 1.

(A) The expression level of LincU is dramatically reduced during differentiation. Data are shown as the mean ± SEM (n=3), ***p<0.001, t-test.

(B) mRNA analysis of nuclear and cytoplasmic fractions of naïve state mESCs showing that LincU is mainly located in the cytoplasm. *Xist* and *Gapdh* serve as positive ctrl of nuclear and cytoplasm, respectively.

(C) Quantitative analysis of western blots in Figure 1C. Data are shown as the mean ±

SEM (n=3), **p<0.01, ***p<0.001, t-test.

(D and E) Colony formation assay using single shCtrl or shLincU cells 48 h after Epiblast induction. Colonies were stained for AP activity on day 6 of culture in the LIF+FBS condition (D) and deemed as either AP-positive or AP-negative (E). Data are shown as the mean ± SEM (n=3), *p<0.05, $^{\#}p$<0.05, t-test.

(F) Validation of the LincU$^{-/-}$ mESC line by PCR genotyping.

(G) Quantitative analysis of western blots in Figure 1G. Data are shown as the mean ± SEM (n=3), *p<0.05, **p<0.01, t-test.

Figure S2. LincU is both essential and sufficient for maintaining the naïve pluripotency of mESCs. Related to Figure 1.

(A) LincU$^{-/-}$ mESCs fail to form chimeras. Scale bar, 2 mm.

(B) Percentage of GFP-positive cells in chimera mice.

(C) Teratoma formation assay by subcutaneously injecting Ctrl and LincU$^{-/-}$ mESCs into the backs of NOD/SCID mice respectively. Four weeks post the injection, teratomas were dissected, photographed (left panel) and weighed (right panel). The ruler scales are 0.1 mm per minor mark. Data are shown as the mean ± SEM (n=3), **p<0.01, t-test.

(D) Relative mRNA levels of primed state-related and developmental genes in the teratomas formed by Ctrl and LincU$^{-/-}$ mESCs were evaluated using qPCR. Data are

shown as the mean ± SEM (n=3), *p<0.05, **p<0.01, ***p<0.001, t-test.

(E) Quantitative analysis of western blots in Figure 1I. Data are shown as the mean ± SEM (n=3), **p<0.01, ***p<0.001, t-test.

(F and G) Colony formation assay for single Ctrl or LincU-overexpressing cells 48 h after Epiblast induction. Colonies were stained for AP activity on day 6 of culture in the LIF+FBS medium (F) and deemed as either AP-positive or AP-negative (G). Data are shown as the mean ± SEM (n=3), **p<0.01, $^{\#\#}p$<0.01, t-test.

(H) Teratoma formation assay by subcutaneously injecting stably lentiviral transfected Ctrl mESCs and LincU-overexpressing mESCs into the backs of NOD/SCID mice respectively. Four weeks post the injection, teratomas were dissected, photographed (left panel) and weighed (right panel). The ruler scales are 0.1 mm per minor mark. Data are shown as the mean ± SEM (n=3), *p<0.05, t-test.

(I) Relative mRNA levels of primed state-related and developmental genes in the teratomas formed by Ctrl and LincU-overexpressing mESCs were evaluated using qPCR. Data are shown as the mean ± SEM (n=3), *p<0.05, **p<0.01, ***p<0.001, t-test.

Figure S3. LincU specifically inhibits the MAPK-ERK signaling pathway. Related to Figure 2.

(A) GO analysis of biological processes associated with differentially expressed genes. The upper panel shows 2097 genes with two-fold upregulated expression and the

lower panel shows 2301 genes with downregulated expression after LincU knockdown.

(B) GO analysis of biological processes associated with differentially expressed genes. The upper panel shows 1506 genes with two-fold upregulated expression, and the lower panel shows 1764 genes with downregulated expression after LincU overexpression.

(C) KEGG analysis of LincU-overexpressing mESCs.

(D-F) Quantitative analysis of western blots in Figure 2I (D), 2J (E), and 2K (F). Data are shown as the mean ± SEM (n=3), *p<0.05, **p<0.01, t-test.

(G) Western blot (n=3) showing higher levels of ERK1/2 phosphorylation in teratoma formed by LincU$^{-/-}$ mESCs.

(H) Quantitative analysis of western blots in Figure S3G. Data are shown as the mean ± SEM (n=3), *p<0.05, t-test.

(I) Western blot (n=3) showing reduced levels of ERK1/2 phosphorylation in teratoma formed by LincU-overexpressing mESCs.

(J) Quantitative analysis of western blots in Figure S3I. Data are shown as the mean ± SEM (n=3), **p<0.01, t-test.

(K) Quantitative analysis of western blots in Figure 2M. Data are shown as the mean ± SEM (n=3), *p<0.05, **p<0.01, $^{\#}p$<0.05, $^{\#\#}p$<0.01, t-test.

Figure S4. LincU stabilizes the ERK-specific phosphatase DUSP9 in mESCs. Related to Figure 3.

(A-C) Quantitative analysis of western blots in Figure 3B (A), 3C (B), and 3D (C). Data are shown as the mean ± SEM (n=3), *p<0.05, ***p<0.001, t-test.

(D) Western blot (n=3) showing reduced levels of DUSP9 in teratoma formed by LincU$^{-/-}$ mESCs.

(E) Quantitative analysis of western blots in Figure S3D. Data are shown as the mean ± SEM (n=3), *p<0.05, t-test.

(F) Western blot (n=3) showing higher levels of DUSP9 in teratoma formed by LincU-overexpressing mESCs.

(G) Quantitative analysis of western blots in Figure S3F. Data are shown as the mean ± SEM (n=3), *p<0.05, t-test.

(H) Crosslinked RIP assay showing the interaction between DUSP9 and LincU. Data are shown as the mean ± SEM (n=3), **p<0.01, t-test. Linc1548 serves as a negative control.

(I-K) Quantitative analysis of western blots in Figure 3I (I), 3J (J), and 3K (K). Data are shown as the mean ± SEM (n=3), *p<0.05, $^{\#}p$<0.05, t-test.

Figure S5. LincU is the direct target of NANOG in naïve-state mESCs. Related to Figure 4 and Figure 5.

(A and B) Quantitative analysis of western blots in Figure 4A. Data are shown as the mean ± SEM (n=3), **p<0.01, $^{\#}p$<0.05, $^{\#\#}p$<0.01, t-test.

(C) Quantitative analysis of western blots in Figure 4C. Data are shown as the mean ± SEM (n=3), ** p<0.01, $^{\#\#}p$<0.01, t-test.

(D) Luciferase reporter assay indicating that the expression of LincU is activated by *Nanog*, *Klf4* and *Smad1*. *p<0.05, ** p<0.01, t-test, n=3.

(E and F) Quantitative analysis of western blots in Figure 5E (E) and 5H (F). Data are shown as the mean ± SEM (n=3), *p<0.05, **p<0.01, $^{\#}p$<0.05, $^{\#\#}p$<0.01, t-test.

Figure S6. Functional role of LincU is conserved in hESCs. Related to Figure 6.

(A and B) Quantitative analysis of western blots in Figure 6D (A) and 6G (B). Data are shown as the mean ± SEM (n=3), *p<0.05, **p<0.01, t-test.

SUPPLEMENTAL TABLE

Table S1. Primers list, related to EXPERIMENTAL PROCEDURES section

Application	**Gene**	**Species**	**Forward primer**	**Reverse primer**
qPCR	*Gapdh*	Mouse	ATGACATCAAGAAGGTGGTG	CATACCAGGAAATGAGCTTG
qPCR	*LincU*	Mouse	AGTGAGGTGGTTTAGTGGAACC	GTGAGTTAGAGCAAGGAGGGC
qPCR	*Rex1*	Mouse	GGAAGAAATGCTGAAGGTGGAGAC	AGTCCCCATCCCCTTCAATAGC
qPCR	*Esrrb*	Mouse	GACCTTTACCGAGCCATCCT	GCCTCCAGGTTCTCAATGTA
qPCR	*Nanog*	Mouse	ATTCTTCCACCAGTCCCAA	ATCTGCTGGAGGCTGAGG

			A	TA
qPCR	*Tcf1*	Mouse	TGGCCTCACTAGAACAAGAGG	CTCGGTCAAGGATGGAAGC
qPCR	*Fgf5*	Mouse	AAAGTCAATGGCTCCCACGAA	GGCACTTGCATGGAGTTTTCC
qPCR	*Dnmt3b*	Mouse	CTCGCAAGGTGTGGGCTTTTGTAAC	CTGGGCATCTGTCATCTTTGCACC
qPCR	*Eomes*	Mouse	CCCTATGGCTCAAATTCCAC	CCAGAACCACTTCCACGAAA
qPCR	*Nestin*	Mouse	GAATGTAGAGGCAGAGAAAACT	TCTTCAAATCTTAGTGGCTCC
qPCR	*Mixl1*	Mouse	ACTTTCCAGCTCTTTCAAGAGCC	ATTGTGTACTCCCCAACTTTCCC
qPCR	*N-cad*	Mouse	TCCTGATATATGCCCAAGACAA	TGACCCAGTCTCTCTTCTGC
qPCR	*Gata4*	Mouse	CCTGGAAGACACCCCAATCTC	AGGTAGTGTCCCGTCCCATCT
qPCR	*Dusp9*	Mouse	CCCCATCTCTGACCATTGGA	TGCGACAAGGCCTCATCAA
qPCR	*Linc1548*	Mouse	GGAGTTGATTTCAGACTATG	TGCAGCAAGTTCTTGTTATC
qPCR	*Med14*	Mouse	AAGGAAACAGGAGATGGGCG	CAGAAGCTGGCAAAGGAGGA
qPCR	*Parp*	Mouse	ACTCATGCTACCACGCACAA	CTTTGACACTGTGCTTGCCC
qPCR	*Erf*	Mouse	ACTGACAAGAGCAGTGGTGG	CTCACCCTCATCTTCAGGGC
qPCR	*Egr1*	Mouse	CCCACCATGGACAACTACCC	GGAGAAGCGGCCAGTATAGG
qPCR	*C-Jun*	Mouse	TGCAAGCCCTGAAGGAAGAG	GCTGCGTTAGCATGAGTTGG
qPCR	*Ubf*	Mouse	GAGACTATCTGGCCCGCTTC	TGCACCTTGTACTGCCTCTG
qPCR	*Brf1*	Mouse	AGCTGGGGAGGCTATTGAGA	ATGGCTTGATTGGCTCTGCT
qPCR	*Sap1*	Mouse	GTTCCTCTTGCACTTGCTGC	AGGACTAAGGCTGCTCCAGA
qPCR	*Sap2*	Mouse	ACCCCAGCCTCCATATCCAT	GCTGGTGTAAGAGACGCTGT
qPCR	*Dvl1*	Mouse	GACAATGCCAAGTTGCCCTG	CGGCTCGTATTGTCCTCCTC
qPCR	*Gsk3β*	Mouse	TGTATGGTCTGCAGGCTGTG	GTTTGACATTTGGGTCCCGC

qPCR	*Wisp*	Mouse	TGATGACGCAAGGAGACCAC	GTACTTGGGTCGGTAGGTGC
qPCR	*Lef1*	Mouse	GGGACCCTCCTACTCCAGTT	TGCCTTGCTTGGAGTTGACA
qPCR	*Dvl3*	Mouse	CATGAGCAACGATGACGCAG	CCGAGCCGATGAAAGCATTG
qPCR	*Tcf3*	Mouse	CCCCAACTACGATGCAGGTC	ATCCTCTTTCTCCTCCCGCT
qPCR	*β -Catenin*	Mouse	GCTGAAGGTGCTGTCTGTCT	GGCAGGCTCAGTGATGTCTT
qPCR	*Tcf7*	Mouse	AGTGCACACTCAAGGAGAGC	TTTCCCTTGACCGCCTCTTC
qPCR	*Lrp6*	Mouse	CAGCATTGAACGTGCCAACA	TCCGAAGGCTGTGGATAGGA
qPCR	*Human LincU*	Human	TCAGATTGGGTTACCACGGG	TTTGGGTGAGGCTGAATCCC
qPCR	*ID3*	Human	CTACAGCGCGTCATCGACTA	TCGTTGGAGATGACAAGTTCC
qPCR	*ZIC1*	Human	GCGCTCCGAGAATTTAAAGA	GTCGCTGCTGTTAGCGAAG
qPCR	*TFE3*	Human	TGCCTGTGTCAGGGAATCTG	CGACGCTCAATTAGGTTGTGAT
qPCR	*MIXL1*	Human	AGCTGCTGGAGCTCGTCTT	CGCCTGTTCTGGAACCATAC
qPCR	*EOMES*	Human	CGCCACCAAACTGAGATGAT	CACATTGTAGTGGGCAGTGG
ChIP-PCR	*Primer#1*	Mouse	GGTGCTCTAACCACTGCCAA	ACAGGCTTACAGCAGACTCA
ChIP-PCR	*Primer#2*	Mouse	CCCGGCACACCTGATCAATA	TCCAGGATGTCCCACTCACA
ChIP-PCR	*Prdm14*	Mouse	GCATCAGGAGATTGCCCCTT	GCTGTGTGAGGTCCTCTGTG
ChIP-PCR	*Negtive control*	Mouse	AGGAGACCAGAGAGGCAAGA	GTCTTGAGGCCAGAAACCTC

SUPPLEMENTAL EXPERIMENTAL PROCEDURES

ESC culture

The mESC line 46C was cultured in DMEM (Gibco) supplemented with 15% FBS (Gibco), 0.1 mM 2-mercaptoethanol (Gibco), 0.1 mM MEM nonessential amino

acids (NEAA, Gibco), 2 mM L-glutamine (Gibco), 1% sodium pyruvate (Gibco), and 1000 units/mL recombinant LIF (Millipore) on feeder cells.

Naïve mESCs were induced by DMEM/F12 (Gibco) and neurobasal medium (Gibco) mixed at a ratio of 1:1 containing 1× B27 (Gibco), 1×N2 (Gibco), 2 mM L-glutamine (Gibco), 0.1 mM 2-mercaptoethanol (Gibco), and 1% knockout serum replacement (KOSR, Gibco) with 3 μM CHIR99021 (Tocris) and 1 μM PD0325901 (Tocris) and LIF (Millipore).

Human ES cell were cultured in DMEM-F12 (Gibco) containing 15% knockout serum replacement (KOSR, Gibco), 1 mM glutamine (Gibco), 1% nonessential amino acids (NEAA, Gibco), 0.1 mM β-mercaptoethanol (Gibco), and 8 ng/ml bFGF (R&D).

Naïve hESCs were cultured in knockout DMEM (Gibco), 1% BSA (Amresco), 1 × N2 supplement (Gibco), 12.5 μg/ml insulin (Roche), 1000 units/mL recombinant LIF (Millipore), 8 ng/ml bFGF (R&D), 1 ng/ml TGF-β1 (Peprotech), 1 mM glutamine (Gibco), 1% nonessential amino acids (Gibco), 0.1 mM β-mercaptoethanol (Gibco), penicillin-streptomycin (Gibco) and small molecule inhibitors: 1 μM PD0325901 (Tocris), 3 μM CHIR99021 (Tocris), 10 μM SP600125 (Tocris) and 10 μM SB203580 (Tocris). All cells were free of mycoplasma contamination.

Plasmid construction

The cDNA sequence of mouse LincU was amplified from 46C ESCs cDNAs. For knockdown experiments, two shRNAs targeting LincU (shLincU-1, 5'-AAGATTCAGCCTCACCAAAAA-3'; shLincU-2,

5’-TTGGCAGGTAGGGTAAGAAAA-3’), one shRNA targeting *Dusp9* (5’-AGTCAGCATCCCACTCTTCTT-3’) and one shRNA targeting *Nanog* (5’-TTAACCTGCTTATAGCTCAGG-3’) were cloned into the pLKO.1-TRC cloning vector obtained from David Root (Addgene plasmid #10878)(Moffat et al., 2006). A shRNA targeting luciferase was also designed as a control (shCtrl, 5’-TGAAACGATATGGGCTGAATA-3’).

To knockout LincU, two guide RNAs (gRNAs) targeting full-length LincU were designed (LincU KO gRNA#1, 5’-CCGGCACACCTGATCAATAA-3’; LincU KO gRNA#2, 5’-CCTTGATCCGAAAGCACCC-3’) and cloned as previously described(Aparicio-Prat et al., 2015). Two gRNAs together with a CAS9 plasmid and puromycin resistance cassette were electroporated into mESCs. We selected the cells with 3-10 μg/ml puromycin for 3 days and the surviving clones were picked up for genomic DNA PCR analysis.

For constitutive overexpression of LincU, a guide RNA (gRNA) targeting a region close to the stop codon of Rosa26 (Rosa26 gRNA: AAGGGTCCTCCTACGTTGT) and a donor plasmid containing S2A-puromycin^{R}-pA-CAG-LincU-pA cassettes (forward primer: 5’-CAAGGTCAGAAGAGTTGGATGC-3’; reverse primer: 5’-ATTAAATGTTGTCCTTTATAAGAGTTGCC-3’) flanked by the 5’ and 3’ homologous arms were co-electroporated into 46C mESCs in a 0.4-cm cuvette (Phenix Research Products) using the Gene Pulser Xcell System (Bio-Rad) at 320 V and 200 μF, and the cells were selected with 5 μg/ml blasticidin (InvivoGen) for 7

days. The surviving clones were selected for genomic DNA PCR analysis.

For lentiviral packaging, HEK 293FT cells (1 well of a 6-well plate) were transfected with foreign DNA (2 μg) together with Pax2 (1.5 μg) and Vsvg (1 μg) using XtremeGENE HP (Roche) according to the manufacturer's recommendations. The supernatant was gently mixed with lentivirus and added to mESCs together with 8 μg/ml polybrene.

To generate inducible human LincU-overexpressing hESC lines, we amplified the sequence at Homo chr16:9453451-9454070 (hg19), which is homologous to the mouse genome. The cDNA sequence (forward primer: 5'-CCTTCAGCTCCATTTTCCCAA-3'; reverse primer: 5'-GTTTTCCCTCCAACACTTACC-3') was amplified from H9 hESCs and cloned into pLVX-Tight-Puro vector, which is a doxycycline-induced overexpression vector. The plasmid was then packaged into lentivirus and concentrated by ultracentrifugation. The viral particles were incubated with the advanced rtTA-expressed hESC line (Li et al., 2017).

Reverse transcription and PCR analyses

Total RNAs were isolated using Trizol (Invitrogen), and reverse transcription into cDNA was performed using the SuperScript III First-Strand Synthesis System (Invitrogen) following the manufacturer's instructions. The cDNAs were subjected to q-PCR (Bio-Rad, CFX Connect Real-Time System) amplification with SYBR Premix Ex Taq (TaKaRa). The primer sequences used for qPCR were listed in Table S1. In

addition, relative gene expression analysis using qPCR was performed with QuantStudio7.

Western blot

We removed the feeder and harvested floating cell populations by centrifugation at 4℃ with 2,000 rpm for 5 min, and protein concentrations were then standardized with the Pierce BCA Protein Assay Kit (Thermo Scientific). In total, 15 μg of total protein was separated by SDS-PAGE, transferred to nitrocellulose membranes, and incubated with primary antibodies. The primary antibodies included DNMT3B (Abcam, #ab122932), N-CADHERIN (BD Biosciences, #610920), GAPDH (Santa Cruz, #SC-47724), p-ERK1/2 (CST, #4370s), ERK1/2 (CST, #4695s), p-MEK1/2 (Bioworld, #BS4733), DUSP9 (Bioworld, #BS2348) and NANOG (Abcam, #ab80892).

Nuclear and cytoplasmic extraction

mESCs were harvested after removing the feeder cells, and 2×10^6 mESCs were transferred to 1.5-mL microcentrifuge tubes and subjected to the NE-PER Nuclear and Cytoplasmic Extraction Kit (Thermal Fisher Scientific) according to the manufacturer's instructions.

Teratoma formation and generation of chimeras

For teratoma formation, mESCs were dissociated and suspended in DMEM at 1×10^7 cells/ml. A total of 1×10^6 cells were subcutaneously injected into NOD/SCID mice. Four weeks post injection, the teratomas were dissected and weighed. Three

biological and three technical replicates were performed for each experiment. Differences in the mean weights in the same individuals were statistically evaluated by Student's t-test.

To generate chimeras, LincU$^{-/-}$ and Ctrl mESCs were first transfected with GFP lentivirus, and the pure 46C-GPF and LincU$^{-/-}$ mESCs were sorted for injection. Then, E2.5 embryos were produced by the electrofusion of 2-cell-stage embryos that were collected from ICR mice and approximately 15 mESCs were injected into the blastocoel cavity using a piezo-actuated microinjection pipette.

FACS analysis

Cells were trypsinized, washed twice with PBS and resuspended in a total volume of 200 μl. Large clumps of cells were removed using a cell strainer (BD Biosciences), then the remaining cells were analyzed by using BD FACSVerse.

Fluorescence-activated cell-sorting analysis

The ESCs transfected with GFP lentivirus and cultured under the serum+LIF condition were trypsinized, washed with PBS, and then collected by centrifugation. Large clumps of cells were removed using a cell strainer (BD Biosciences). The cells were sorted and analyzed on a flow cytometer (ARIA II; BD Biosciences). The GPF fluorescence activities were detected in the FITC channel.

mRNA microarray analysis

For microarray analysis in shLincU-2 and shCtrl mESCs, total RNA was quantified by a NanoDrop ND-2000 (Thermo Scientific), and the RNA integrity was

assessed using Agilent Bioanalyzer 2100 (Agilent Technologies). Sample labeling, microarray hybridization and washes were performed based on the manufacturer's standard protocols. Briefly, total RNA was transcribed into double-stranded cDNA, which was then synthesized into cRNA and labeled with Cyanine-3-CTP. The labeled cRNAs were hybridized onto the microarray. After washing, the arrays were scanned by the Agilent Scanner G2505C (Agilent Technologies). Feature Extraction software (version10.7.1.1, Agilent Technologies) was used to analyze array images to obtain the raw data. Genespring (version13.1, Agilent Technologies) was employed to finish the basic analysis of the raw data. First, the raw data was normalized with the quantile algorithm. The probes with at least 100% of the values in any one condition and flags indicating "detected" were chosen for further data analysis. Differentially expressed genes were then identified based on fold changes. The threshold set for up- and downregulated genes was a fold change≥2.0. Afterwards, GO analysis and KEGG analysis were applied to determine the roles of these differentially expressed mRNAs.

For microarray analysis in LincU-overexpressing and Ctrl mESCs, total RNA was checked for a RIN number to inspect RNA integrity by an Agilent Bioanalyzer 2100 (Agilent technologies, Santa Clara, CA, US). Qualified total RNA was further purified by a RNeasy micro kit (Cat#74004, QIAGEN, GmBH, Germany) and RNase-Free DNase set (Cat#79254, QIAGEN, GmBH, Germany). Total RNA was amplified, labeled and purified by using the GeneChip 3' IVT PLUS Reagent Kit (Cat#902416, Affymetrix, Santa Clara, CA, US) following the manufacturer's instructions to obtain biotin-labeled cRNA. Array hybridization and washes were

performed using the GeneChip Hybridization Wash and Stain Kit (Cat#900720, Affymetrix, Santa Clara, CA, US) in a Hybridization Oven 645 (Cat#00-0331-220V, Affymetrix, Santa Clara, CA, US) and Fluidics Station 450 (Cat#00-0079, Affymetrix, Santa Clara, CA, US) following the manufacturer`s instructions. Slides were scanned by a GeneChip Scanner 3000 (Cat#00-00212, Affymetrix, Santa Clara, CA, US) and Command Console Software 4.0 (Affymetrix, Santa Clara, CA, US) with default settings. Raw data were normalized by the MAS 5.0 algorithm using Gene Spring Software 11.0 (Agilent technologies, Santa Clara, CA, US).

GO analysis

GO enrichment was carried out using the DAVID functional annotation bioinformatics microarray analysis tool (https://david.ncifcrf.gov/).

Native RIP Assay and crosslinked RIP assay

For native RIP assay, 5×10^6 ESCs were harvested after removing the feeder cells, lysed in 0.2 mL of lysis buffer [100 mM KCl, 5 mM $MgCl_2$, 10 mM HEPES (pH 7.0), 0.5% Nonidet P-40, 1 mM dithiothreitol] containing protease inhibitors and an RNase inhibitor (Promega) and centrifuged at 13，000 rpm for 10 min. The supernatants were incubated with anti-DUSP9 (Bioworld, #BS2348) and anti-rabbit IgG (Millipore, 12-370) for 6 h at 4℃ with gentle rotation. Next, 15 μL of Protein G Dynabeads (Invitrogen) was added, and the mixture was incubated for 3 h at 4℃ with gentle rotation. The beads were washed three times with wash buffer [50 mM Tris (pH 7.4)], 1 mM $MgCl_2$, 150 mM NaCl, 0.05% Nonidet P-40) containing an RNase inhibitor

(Promega) and twice with PBS containing an RNase inhibitor (Promega). RNA was extracted using a total RNA isolation kit (TIANGEN), and qPCR was performed as described above. Primer sequences for qPCR are listed in Table S1.

For crosslinked RIP assay, 5×10^6 ESCs were harvested after removing the feeder cells, crosslinked with 1% formaldehyde for 10 min at RT, and quenched with 0.125 M glycine. Then, the lysed samples were washed twice with cold PBS. The remaining steps were the same as those in native RIP assay.

Chromatin immunoprecipitation (ChIP) assays

ChIP assays were performed as previously described (Li et al., 2017). Briefly, mESCs were harvested after removing the feeder cells, crosslinked with 1% formaldehyde for 10 min at RT, and quenched with 0.125 M glycine. The lysed samples were washed with PBS twice and sonicated to generate DNA fragments approximately 500 bp in length. Then the chromatin fragments were immunoprecipitated at 4℃ overnight with anti-NANOG (1:2000, Abcam, #ab80892) and Rabbit IgG. After dissociation from the immune complexes, the immunoprecipitated DNAs were quantified by qPCR and normalized against the genomic DNA input prepared before immunoprecipitation. The primers used in ChIP-qPCR analysis were listed in Table S1.

Luciferase reporter gene assay

LincU promoters sequence (-919 bp to -217 bp away from the TSS of LincU) was cloned into pGL3 vector (forward primer: 5’-ACACAAGTCCTTGGTCGGC-3’;

reverse primer: 5’-CAGCTGACTTTTTCTTTCCCC-3’). For mutant LincU promoter, we deleted two possible *Nanog* binding motifs (AGACCATCCCC; GGCTAATTACC) in LincU promoter, and the mutant LincU promoter sequence was synthesized by RuiDi Biological Technology Company. NIH/3T3 cells were cultured in DMEM supplemented with 10% FBS. In total, 5×10^4 cells well were plated in one well of 24-well plate and transfected with Opti-MEM (1:100 μl), 10 ng of Renilla luciferase and 200 ng of the pGL3 luciferase reporter were co-transfected with Ctrl vector, *Nanog*, *Sox2*, *Esrrb*, *Klf4*, *Smad1* overexpression plasmid with Lipofectamine 2000 (Invitrogen). The luciferase assays were performed using the Dual-Luciferase Reporter Assay System (Promega).

Reference

Aparicio-Prat, E., Arnan, C., Sala, I., Bosch, N., Guigo, R., and Johnson, R. (2015). DECKO: Single-oligo, dual-CRISPR deletion of genomic elements including long non-coding RNAs. BMC Genomics *16*, 846.

Karwacki-Neisius, V., Goke, J., Osorno, R., Halbritter, F., Ng, J.H., Weisse, A.Y., Wong, F.C., Gagliardi, A., Mullin, N.P., Festuccia, N., *et al.* (2013). Reduced Oct4 expression directs a robust pluripotent state with distinct signaling activity and increased enhancer occupancy by Oct4 and Nanog. Cell Stem Cell *12*, 531-545.

Li, G., Jiapaer, Z., Weng, R., Hui, Y., Jia, W., Xi, J., Wang, G., Zhu, S., Zhang, X., Feng, D., *et al.* (2017). Dysregulation of the SIRT1/OCT6 Axis Contributes to Environmental Stress-Induced Neural Induction Defects. Stem Cell Reports *8*, 1270-1286.

Moffat, J., Grueneberg, D.A., Yang, X., Kim, S.Y., Kloepfer, A.M., Hinkle, G., Piqani, B., Eisenhaure, T.M., Luo, B., Grenier, J.K., *et al.* (2006). A lentiviral RNAi library for human and mouse genes applied to an arrayed viral high-content screen. Cell *124*, 1283-1298.